Investigating Coastal Groundwater Discharge from the Willunga Basin, using hydrogeophysical techniques.

Marianna Ramirez Lagunas

Supervisors: Dr. Ilka Wallis

Dr. Edward Banks

Dr. Margaret Shanafield

Thesis submitted in partial requirement for the degree of Master of Science (Groundwater Hydrology)

College of Science and Engineering

Flinders University

16 October 2017

CONTENTS

LIST OF FIGURES

LIST OF TABLES

SUMMARY

Coastal groundwater discharge (CGD) is a noteworthy source of freshwater and nutrients to oceans. It is acknowledged as an important component in groundwater budget calculations and in freshwater-seawater interaction studies. Nevertheless, information regarding CGD is still limited due to the difficulty in identifying discharge zones and the complex processes that control this phenomenon.

This study aims to identify CGD zones occurring as freshwater seeps, in Sellicks Beach, South Australia, located in the south-western part of the Willunga Basin. The basin comprises a multi aquifer system that provides freshwater to the McLaren Vale region. Limited hydrogeological information available from the coastal area of this Basin has resulted in the misinterpretation of the discharge to the sea component of the water balance of the Willunga Basin. To assess the CGD at Sellicks Beach a number of methods have been used in this study. A discharging site (seep) was located and analysed by piezometers at, and in proximity, to the site. A range of different investigative techniques provided considerable insight into the subsurface processes. These techniques included stable environmental isotopes to investigate the origin of the discharging water. In order to examine the composition of the water, the water level fluctuation and water temperature, hydrochemistry analyses were conducted at Sellicks Beach. A near surface geophysical survey to obtain the spatial distribution of the ground conductivity and thermal imagery to locate the freshwater seeps and their alleged preferential flowpaths.

The piezometers measurements indicated that the average temperature of the water at a discharging site (~18.5 °C) was higher than that of the sites where no discharge was visible (~ 16.4 °C). Additionally, the water level measurements showed the highest

upward gradient at the discharging site. The hydrochemistry assessment indicates that the water at the visible discharging site is composed of freshwater and that during high tide periods is influenced by seawater. These results suggested that the water at the discharging site can be associated to freshwater and also correlates to the tidal cycle variations.

The near surface geophysical survey provided a 3D resistivity model that along with the previous methods, showed the groundwater flowing towards the sea. The thermal imagery was able to identify three additional discharging sites in the surrounding area. The temperature registered with the thermal images indicated that the water flows at~ 18-19 °C, these values are supported by the temperate results obtained with the piezometers and indicate the presence of groundwater. This method was also able to identify a preferential flowpath towards the sea.

Even though the techniques applied in this study are reasonably different, the results are consistent and revealed the presence of CGD at Sellicks Beach, as it was confirmed that the use of multiple techniques provides a good way to understand near surface water flow in coastal environments.

DECLARATION

I certify that this thesis does not incorporate without acknowledgment any material previously submitted for a degree or diploma in any university; and that to the best of my knowledge and belief it does not contain any material previously published or written by another person except where due reference is made in the text.

Signed Marianna Ramirez Lagunas.

Date

21/November/2017

ACKNOWLEDGEMENTS

I would like to thank my supervisors Ilka Wallis, Eddie Banks and Margaret Shanafield for their valuable support, guidance, patience and helpful advice during this project. I highly appreciate all their efforts and contributions to my research project. I would like to thank Louise Michaud for her help during the fieldwork activities of this research.

To my family for always uplifting my spirit and keeping me on the right track. A special mention to my mom Rebeca and grandma Mamisa for always being there for me, for their motivation, support and affection. Without them I wouldn't have had the courage to come to Australia and pursue this dream.

Additionally, I would like to thank my friends back home in Mexico, my friends and colleagues here in Australia for their constant motivation that helped me go through this wonderful journey. Also, thanks to everyone in the Honours room for their company and friendship.

Editor, Saskia Noorduijn, provided copyediting and proofreading services, according to the guidelines laid out in the university-endorsed national 'Guidelines for editing research theses'.

Chapter 1

Introduction

Groundwater is a substantial component of the water resource systems that supply water for numerous uses, such as domestic and agricultural (Bear and Verruijt, 2012). Studying and understanding the behaviour of groundwater is beneficial to the decision making stage of any water management scheme, and supports the development and operation of any groundwater system (Bear, 2007). The components of a groundwater balance are mainly inflows (may include natural replenishment and artificial recharge) and outflows. The Willunga Basin located in South Australia, provides freshwater to the McLaren Vale region, where wine and other important agricultural industries are established (Harrington and Cook, 2012). This study focuses on the identification of groundwater discharge to the sea that is one of the constituents of the outflow components of the Willunga Basin's multi aquifer system.

Martin (1998) identified discharge to sea and to wells as the principal sources of losses (outflows) from the Willunga Basin aquifer system, however as highlighted by Martin et al (2006) and Short (2011), information regarding groundwater discharge from the Willunga Basin's aquifer system to the Gulf St Vincent is still limited. This represents a major knowledge gap for a clearer understanding of the water balance within the Willunga Basin and thus the sustainability of the resource.

This study is intended to fill this knowledge gap, focusing on investigating freshwaters-seawater interactions in the south-western part of the Basin. The main objective of this study if to identify the presence of coastal groundwater discharge (CGD) at Sellicks Beach and describe its spatial distribution. An additional objective is to show that

geophysical techniques can provide useful information in coastal environments that can help identify groundwater discharge zones.

1.1 Review of literature

Groundwater discharge can be an ambiguous term in the literature (Younger, 1996), Submarine Groundwater Discharge (SGD) can be often defined as the 'direct flow of water into the sea through porous rocks and sediments' (Church, 1996). However, Burnett et al (2003) defined SGD as only involving the offshore discharge of freshwater (Burnett et al., 2003), whilst Johannes (1980) includes in the SGD term the freshwater that flows out along coastal areas (Johannes, 1980). Meanwhile the Coastal Groundwater Discharge (CGD) is commonly defined as the continental groundwaters that flow towards the sea in coastal environments (Burnett et al., 2003).

1.1.1 Coastal groundwater discharge (CGD)

According to Burnett (1999), direct groundwater discharge to the sea occurs as springs and seeps in coastal areas globally and, despite their commonly low discharge rates, the persistent flow through springs and seeps can constitute a volumetrically significant discharge from the groundwater system. Discharge, however, can vary considerably due to tidal fluctuations (Ataie-Ashtiani et al., 2001), highlighting the importance of including tidal fluctuation analysis when assessing groundwater dynamics in coastal areas.

Given the above, groundwater discharge in coastal zones has gained greater attention over the last few years/decades and is now acknowledged as an important process in water balance calculations, and also recognised as a significant conduit for solutes out to sea (Taniguchi et al., 2002). As suggested by Stieglitz (2005), groundwater with its

higher nutrient loading compared to seawater, can provide large amounts of nutrients to the sea despite small fluxes. Other studies highlight the importance of coastal discharge in relation to their contribution to coastal ecology and coastal biodiversity (Li et al. (2008).

A study case by Johannes (1980), investigating discharge features along a sand beach in the lower intertidal zones north of Perth, Western Australia, showed that freshwater discharge (in the lower intertidal zones) to the sea can have a great impact on the ecology of the area and results revealed that groundwater discharge can influence coastal land features by erosion and alter productivity, biomass and species composition.

1.1.2 Submarine groundwater discharge (SGD)

Offshore springs and seeps have been a subject of interest since the era of the Roman Empire (Burnett, 1999). People have been observing these phenomena because they can provide considerable amounts of freshwater, sufficient to satisfy human requirements. Taniguchi et al. (2002) mentioned that the presence of SGD has been known for several years, however it has not been studied in detail, and information regarding the locations of discharge zones tends to be anecdotal. He also mentions that SGD overlooking can be related to the difficulty in locating and measuring it. As stated by Post et al. (2013), offshore groundwater discharge can flow slowly through low permeability confining layers and can extend across widespread regions 'far beyond the coastline' (Figure 1).

Lamontagne et al. (2005) used environmental tracers (Radium and Radon) to measure groundwater discharge along the Gulf St Vincent in South Australia. Their results indicated that discharge of groundwater can be a complex process and that radium can

overestimate groundwater discharge rates. Their findings suggested that SGD can occur as seeps along the entire coastline of the Basin.

Short et al. (2014) collected samples along the coastline of the Willunga Basin to obtain measurements of electrical conductivity and radon that would help in assessing the SGD. Their findings suggested that SGD can occur as seeps along the entire coastline of the Basin.

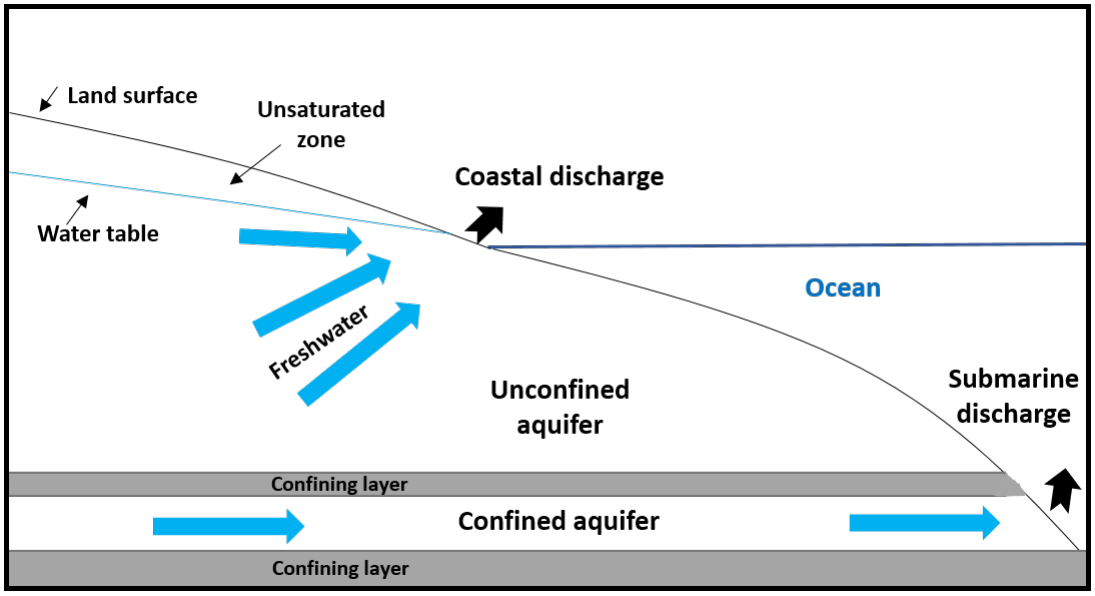

Figure 1 Representation of coastal freshwater discharge and SGD. Modified after (Johannes, 1980).

1.1.3 Geophysical techniques

Post (2005) recognized that in order to obtain an effective hydrogeological characterization, different methods should be applied to obtain information on the lateral variations of the properties being evaluated, he suggests methods such as electrical, electromagnetic and seismic. In addition to these geophysical methods, Burnett et al. (2003) considers the implementation of methods that evaluate isotopic signatures and other chemical properties of water that provide information regarding the origin and physical driving forces of water.

Geophysical techniques that focus on the ground conductivity can be applied to evaluate the spatial distribution of freshwater and seawater (Burnett et al., 2006). Conductivity methods can help in identifying preferential groundwater flowpaths.

A study case in Queensland, Australia by Stieglitz (2005) applied electrical geophysical techniques to analyse groundwater discharge to the sea as seeps in the beach face of Ella Bay. They demonstrated that methods that measure the ground electrical conductivity can provide useful information regarding the location and pathway of groundwater. This is possible given the fact that conductivity can be a function of water salinity and temperature. The results of the conductivity transects showed a well-defined conductivity contrast at low tide that was associated to the freshwater-seawater interface.

Another study in Sicily, Italy by Povinec et al. (2006) measured the electrical properties of the subsurface using a time domain electromagnetic instrument, and was able to locate the freshwater-seawater interface in a coastal environment. They found that the spatial distribution of the measured conductivity correlates to the daily tidal cycle and groundwater fluxes.

In Ubatuba, Brazil, Stieglitz et al. (2008) used a conductivity meter to study the spatial variations of the electrical properties in Flamengo Bay, to assess the groundwater system in the area. Their results showed that subsurface electrical conductivity measurements can identify contrasts in the spatial distribution of the ground conductivity that are associated to preferential discharging groundwater flowpaths.

Another geophysical tracer commonly applied to the studies of freshwater-seawater interaction, is temperature, and it can be measured using infrared sensors (Burnett et al., 2006). As acknowledged by Mundy et al. (2017), 'groundwater has an identifiable

thermal signature, due to its relatively constant temperature' that can be evaluated by a relatively simple and non-invasive method, such as thermal imagery. This method can be effective in the characterization of seeps, even under low flow conditions.

Mulligan and Charette (2006) used airborne thermal imagery, to investigate the spatial variability of groundwater discharge in Waquoit Bay, Massachusetts. The heterogeneous temperature distribution displayed in their thermal images provided evidence of diffuse groundwater discharge along the bay. Their study demonstrated that thermal images are useful in assessing the spatial variability of alongshore groundwater discharge.

Using a ground-based thermal infrared camera, Pfister et al. (2010) was able to characterise a subsurface saturated area. Their study suggested that thermal IR imaging techniques can complement conventional tracer techniques that help identify the connection of groundwater and surface water.

Schuetz and Weiler (2011) used a handheld infrared camera to identify groundwater inflows to downstream discharge in Southwest Germany. They advised that the use of ground-based thermal imagery can provide *in situ* information to determine groundwater discharge and its interactions with surface water.

For the purposes of this study, geophysical surveys that evaluate the electrical conductivity of the ground, and handheld infrared thermal camera to analyse the temperature of the discharging water in the coastal zone, are going to be conducted.

Chapter 2

Study area and background information

2.1 The Willunga Basin

The Willunga Basin is part of the bigger St Vincent Basin, formed during the continental separation of Australia and Antarctica ~43 million years ago (Dyson, 1998, Martin, 1998). The basin is bounded to the east and south by the Willunga Fault, to the north by the Onkaparinga River and to the west by St Vincent's Gulf (Figure 4). It is wedge-shaped and consists principally of mid to late Tertiary and Quaternary sediments (Martin, 1998).

2.1.1 Regional Geology

The Willunga Basin consists predominantly of Tertiary marine fossiliferous strata, and fluvial Quaternary sediments (Fairburn, 1998). A brief description of the geologic settings that gave shape to the Willunga Basin is included below and illustrated in Figure 2. The main stratigraphic units found in the basin are:

- ***Cape Jervis Formation***

  The basement of the Basin, consists of Precambrian and Cambrian highly weathered rocks (Smith et al., 2016). These basement rocks are mainly interbedded slates, quartzites and dolomites (Martin, 1998).

- ***Maslin Sands (North and South)***

  The mid-Miocene Maslin Formations are divided in two, a North and a South Formation. The North Maslin Sand is described as fluvial in origin, consisting of cross-bedded quartz sand and gravel (Dyson, 1998). And Smith et al. (2016)

described the South Maslin Sand as marginal marine in origin, consisting mainly of ferruginous glauconitic quartz sand.

- ***Tortachilla Limestone***

Dyson (1998) identified that the Tortachilla Limestone overlies the South Maslin Sand. Smith et al. (2016) indicated that it consists of basal bryozoal ferruginous sand, overlain by glauconitic fossiliferous limestone.

- ***Blanche Point Formation***

This Formation is described by Dyson (1998) as lagoonal origin, and consisting of multiple members (Tuit, Perkana, Gull and Turketja). The lithological composition of the Blanche Point Formation is mainly of silty sandy clay, glauconitic and calcareous fossiliferous mudstone (Smith et al., 2016).

- ***Port Willunga Formation***

Comprised by two members (Aldinga and Ruwarung) and formed in a marine environment, consists mainly of cross-bedded sands and limestones, mudstone and chert nodules (Dyson, 1998).

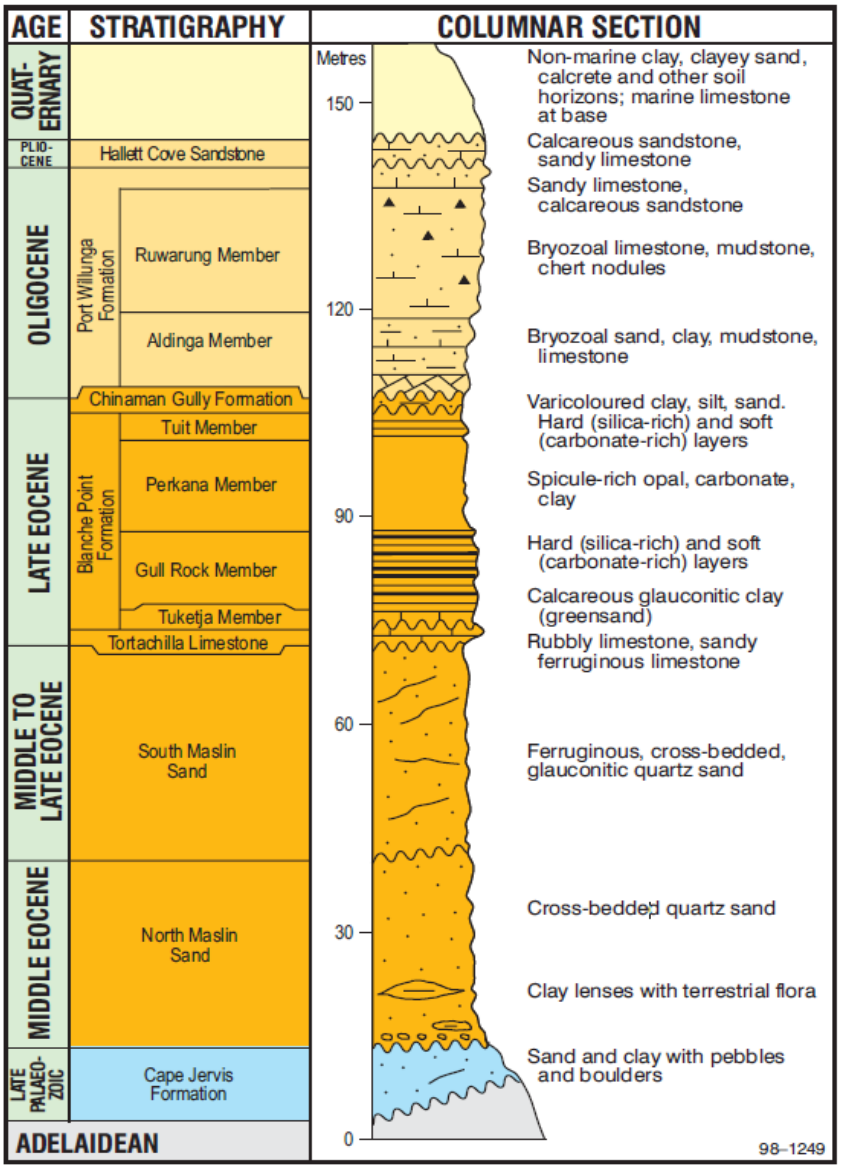

Figure 2 Stratigraphic section of the Willunga Basin (Dyson, 1998).

2.1.2 Geology at Sellicks Beach

The Port Willunga Formation at Sellicks Beach includes bioclastic calcarenites of Miocene age, outcropping as low cliffs and platforms, exposed during low tide (Cann et al., 2014). Sellicks Beach township is located inland of coastal cliffs eroded into alluvial fan sediments consisting of conglomerates, sands and clays (Bourman et al. (2016). These cliffs are susceptible to erosion, deep gullying and slumping. 'The cliffs of Quaternary alluvial fan sediments at Sellicks Beach are an outcome of marine erosion following the postglacial marine transgression and the continuing present high stand of sea-level' (Cann et al., 2014).

The Geological Society of Australia (SA Division) (2014), identified that the present day sediments of the Sellicks Beach area are resultant from continuous erosion and down-slope transport of the alluvial fan sediments in the cliffs at the beach (Figure 3).

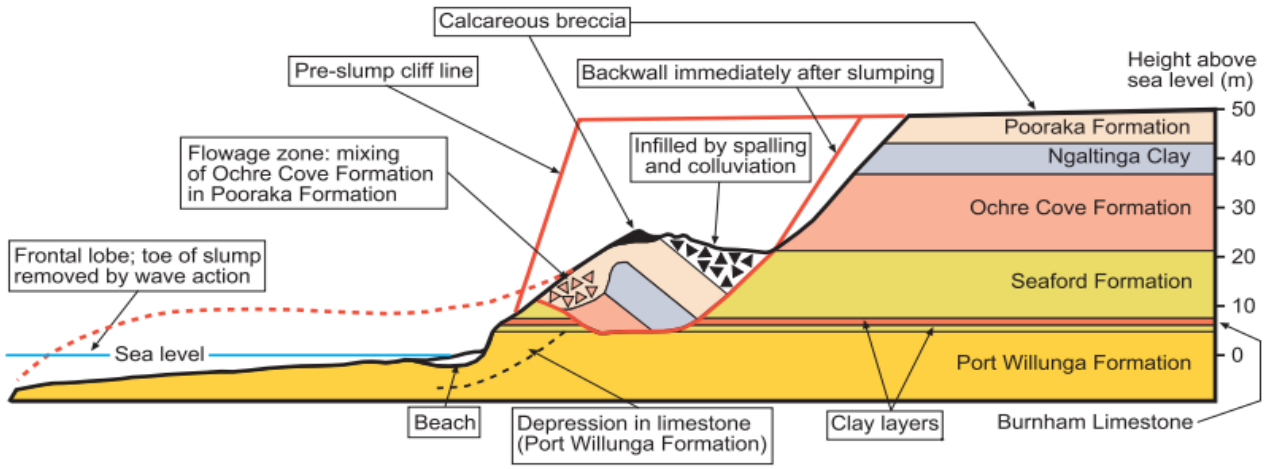

Figure 3 Cross-section at Sellicks Beach (Cann et al., 2014).

The Seaford Formation as described by Fairburn (1998), is a sequence of fluvial origin sand, clay and pebble beds and is exposed in the coastal cliffs of the Sellicks Beach area. The Ochre Cove Formation is also of fluvial origin, comprises sandstone, gravel and conglomerate, and overlays the Seaford Formation. Moreover, the Ngaltinga Clay or

Ngaltinga Formation, comprises clayey sand and clay with infrequent sandy interbeds (Fairburn, 1998).

The sediment transport system at the beach varies seasonally, during winter time the wave energy is usually stronger and gravel deposits are exposed across the beach. The sand during winter is restricted to a thin section exposed only at low tide. Meanwhile, in summer, as the wave energy is usually moderate to low, some of the gravel is covered by a thin layer of sand (Cann et al., 2014).

2.1.3 Hydrogeology and the Willunga Basin's aquifers system

Smith et al. (2016) defined the Willunga Basin as a complex multi-aquifer system within the McLaren Vale Prescribed Wells Area (PWA) (Figure 4). It comprises four main hydrogeological units, the Quaternary, the Port Willunga Formation (PWF), the Maslin Sands and the Fractured Basement Rocks (Table 1).

The Quaternary aquifer is mainly unconfined, and considered as a low yielding aquifer. Therefore, it is generally not used to meet big irrigation demands (Adelaide and Mount Lofty Ranges NRM Board, 2007).

The main sources of groundwater within the basin are the Maslin Sands and PWF aquifers (Martin, 1998). The PWF aquifer is mostly unconfined in the central and eastern part of the Basin. The Maslin Sands aquifer is confined and is commonly considered as lower yielding compared to the PWF aquifer. Rainfall and infiltration through streambeds recharge the Quaternary aquifers. The Maslin Sands and PWF aquifers are recharged through rainfall infiltration, recharge also occurs by streams and lateral inflows from the Fractured Basement Rocks aquifer (Adelaide and Mount Lofty Ranges NRM Board, 2007).

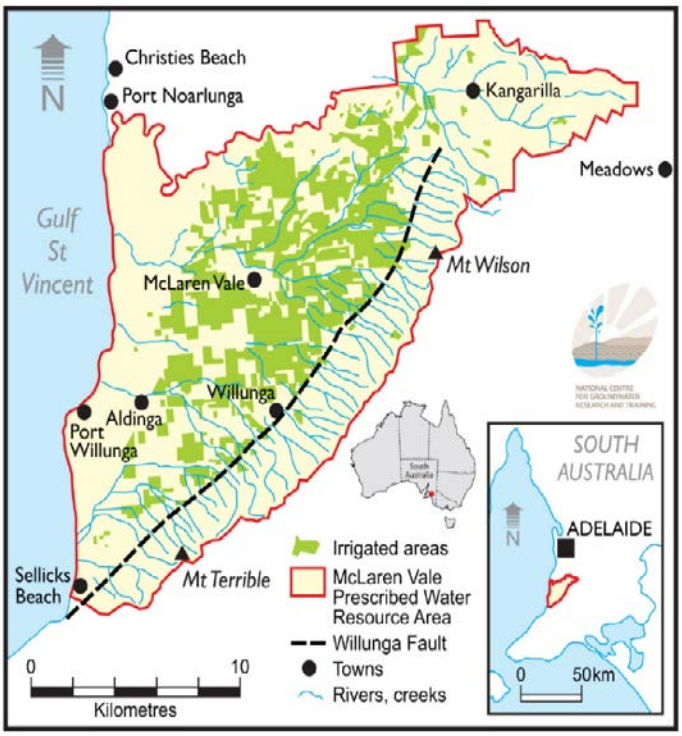

Figure 4 Sellicks Beach and the Willunga Basin, South Australia (Harrington and Cook, 2012).

Anecdotal information from local people has pointed out the presence of groundwater seeps on the beach during low tide in the southeaster part of the Basin. It has been suggested by the Adelaide and Mount Lofty Ranges NRM Board (2007) that in Sellicks Beach these freshwater seeps presumably originate from the perched Quaternary aquifers.

Table 1 Hydrostratigraphy of the Willunga Basin. Modified after Smith et al. (2016) and DfW (2011).

Geological Time			Stratigraphy		
Era	Period	Epoch	Unit	Lithology	Hydroestratigraphy
Cenozoic	Quaternary	Holocene	Semaphore Sands	Thin sand and gravel	Quaternary aquifer
			Ngarkipani Sands	Thin sand	
		Pleistocene	Christies Beach Formation	Fluvial clay with gravel lenses	
			Kurrajong Formation	Thin sand	
			Ngaltinga Formation	Clayey sand and clay with sandy interbeds	
			Pirramimma Sandstone	Sandstone	
			Ochre Cove Formation	Bedded sandstone, gravel and conglomerate	
	Neogene	Oligo-Miocene	Port Willunga Formation	Calcareous sand, clay and silt	Port Willunga Formation Aquifer
	Paleogene	Eocene	Chinaman Gully Formation	Carbonaceous sand, silt and clay	Aquitard
			Blanche Point Formation	Glauconitic, calcareous mudstone, chert, silt and clay	
			Tortachilla Formation	Fossiliferous limestone, basal ferruginous sand	
			South Maslin Sand	Sand, clay and glauconite	Maslin Sands Aquifer
			North Maslin Sand	Poorly sorted sand	
Paleozoic	Permian		Cape Jervis Formation	Shale, Tilite	Aquitard
	Cambrian				
Proterozoic	Neoproterozoic		Adelaidean	Shale, Tilite dolomite, quartzite	Fractured Rocks Aquifer
	Paleoproterozoic				

2.2 Near surface geophysical techniques

A geophysical survey is a measurement made commonly on the earth's surface (Telford et al., 1990). Its main objective is to acquire information of a physical property or properties of the interior of the earth, using measurements of an associated physical field that has originated on the surface of the earth, (West and Macnae (1991). Additionally, Telford et al. (1990) considered important to highlight that geophysical methods can only identify discontinuities or contrasts, that is, where certain physical properties effectively differ from another. According to Butler (2005), near surface geophysical techniques study the physical properties of the shallowest part of the earth's crust and have numerous applications, such as environmental, groundwater, geological, mining, among others. Particularly, geophysical techniques are useful in groundwater studies to assist in mapping water tables, identify possible groundwater contamination, etc. These techniques are characterized by the requirement of high resolution, shallow

targets, and confirmation of results by applying multiple techniques. Other studies have defined the near surface as a multi-component and complex region of the earth. Knowing the properties of these components can provide information to associate the materials of the near surface (minerals, rocks, soil, water, etc.) to the geophysical results and provide an integrated interpretation (Knight and Endres, 2005).

2.2.1 Electromagnetic (EM) method

The EM method is known to respond best to shallow depth electrical conductors and is based on the propagation of low frequency EM fields in and over the earth (Telford et al., 1990). In particular, an EM survey aims to identify the electrical conductivity by measuring the sensed electric and magnetic fields.

As defined by McNeill (1980), electromagnetic Induction (EMI) methods measure the ground apparent electrical conductivity/resistivity. Spies and Eggers (1986) defined the apparent resistivity as 'the resistivity of a homogeneous half-space which will produce the same response as that measured over the real earth with the same acquisition parameters'.

EMI methods are based on an EM field produced by a transmitter coil (Tx) that induces electrical currents in the ground and these currents generate a secondary magnetic field and both fields are sensed by a receiver coil (Rx) (illustrated in Figure 5). Thus, the apparent conductivity (σ_a) can be obtained by measuring the ratio of the secondary (H_s) and primary fields (H_p), as defined from equation (1), from McNeill (1980).

$$\boldsymbol{\sigma_a = \frac{4}{\omega \mu_0 s^2}\left(\frac{H_s}{H_p}\right)} \qquad \textbf{(1)}$$

Where σ_a= apparent ground conductivity

H_p= primary field

H_s = secondary magnetic field

ω= 2*π*Frequency

μ_0=permeability of free space

s= intercoil spacing

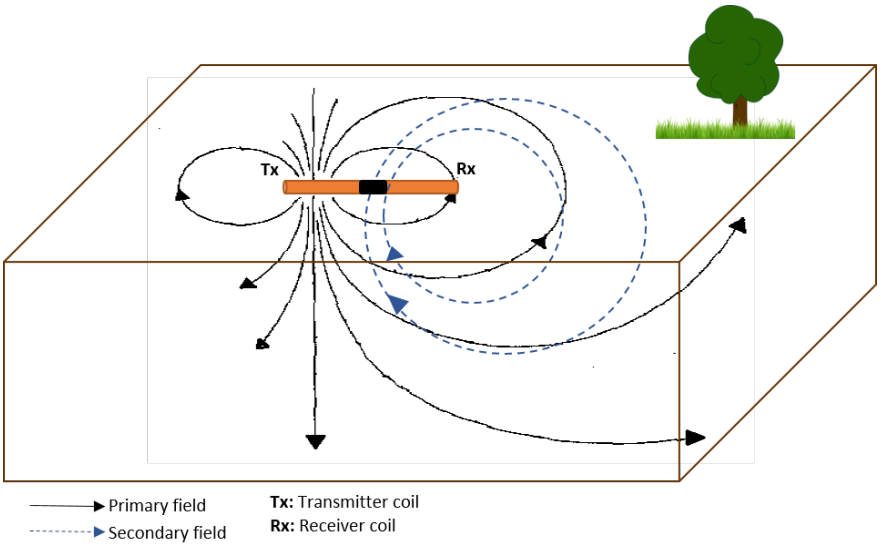

Figure 5 Illustration of the EM method using a contactless geophysical tool.

2.2.1.1 EM methods interpretation

The theoretical basis of all electromagnetic methods used in geophysical prospecting are Maxwell's equations. These linear differential equations describe the behaviour of the EM fields and establish the relationships between the field, the medium and the source (Ward and Hohmann, 1988). When working with EM fields as a wave propagation form, the Maxwell's equation tends to be expressed in the frequency domain. To do that, one must assume time variable harmonic fields, and then substitute the real part of the fields into the Maxwell's equations and convert it to a frequency domain. Another way is to use the Fourier Transform to go from time to frequencies domain.

The study of EM methods consists of the analysis of the data observed by a receiver (Figure 5), and that is known as the *forward problem*. The objective of the observations is to map and interpret the spatial distribution of the physical property being assessed, this is known as the *inverse problem* (Zhdanov, 2002*)*.

2.2.1.2 The electromagnetic conductivity meter

A CMD-Explorer (Figure 6) was used to obtain ground conductivity data. It is a contactless frequency domain EM conductivity meter (GF Instruments, 2016). This instrument provides measurements in two depth ranges (high and low), and are given by the distance between the coil centres of the transmitter and receiver. These high or low depth ranges of investigation can be acquired by modifying the dipole distances or changing the dipole orientation, this orientation can be vertical or horizontal (Instruments, 2016). Additionally, the CMD-Explorer can be programmed for manual or continuous measurements.

Figure 6 CMD-Explorer equipment and user.

EM data collected using the CMD-Explorer can be processed to generate multi-layer maps that represent the spatial distribution of the apparent conductivity/resistivity.

CMD data interpretation was conducted using the commercial software Res2Dinv and Res3Dinv, which are suitable when working with 'structures with fluent resistivity change'. Res2Dinv and Res3Dinv are Windows based programs designed to obtain 2-dimensional and 3-dimensional models, respectively, of the resistivity distribution in the subsurface (Geotomo Software, 2013) . Both programs, when processing CMD-Explorer data assume the Wenner-Schlumberger array. This configuration is an adapted form of the Schlumberger array and is sensitive to horizontal and vertical structures (Yanful, 2009).

2.3 Hydrochemistry

Environmental isotope data can be used in hydrogeological studies to obtain information on type, origin and age of groundwater. The most commonly used environmental isotopes are hydrogen (^{2}H, and ^{3}H) and oxygen (^{18}O) (Aggarwal et al., 2009). The distribution of the stable isotopes, ^{2}H and ^{18}O in groundwater correlates with isotopic data of precipitation and can describe the origin and movement of groundwater (Terwey, 1984). Stable isotope concentrations are normally given as ratios of the least abundant isotope over the most abundant isotope. The ratio is expressed relative to a standard, which, for water, is the "Vienna Standard Mean Ocean Water" (VSMOW). Variations in these ratios within the groundwater system are usually expressed using the δ notation (in per mille units), which relate the isotopic ratio in the groundwater sample to the ratio in the standard. Variations in stable isotope ratios are controlled by chemical reactions and phase changes because of the energy difference between chemical bonds involving different isotopes of an element (Aggarwal et al., 2009).

Chapter 3

Methodology

3.1 Area of study

Sellicks Beach is located approximately 46 km south of Adelaide, South Australia and is situated in the southern part of the Willunga Basin, (see Figure 7). The hydrogeology and geology of the area are briefly described in section 2.1 of this thesis.

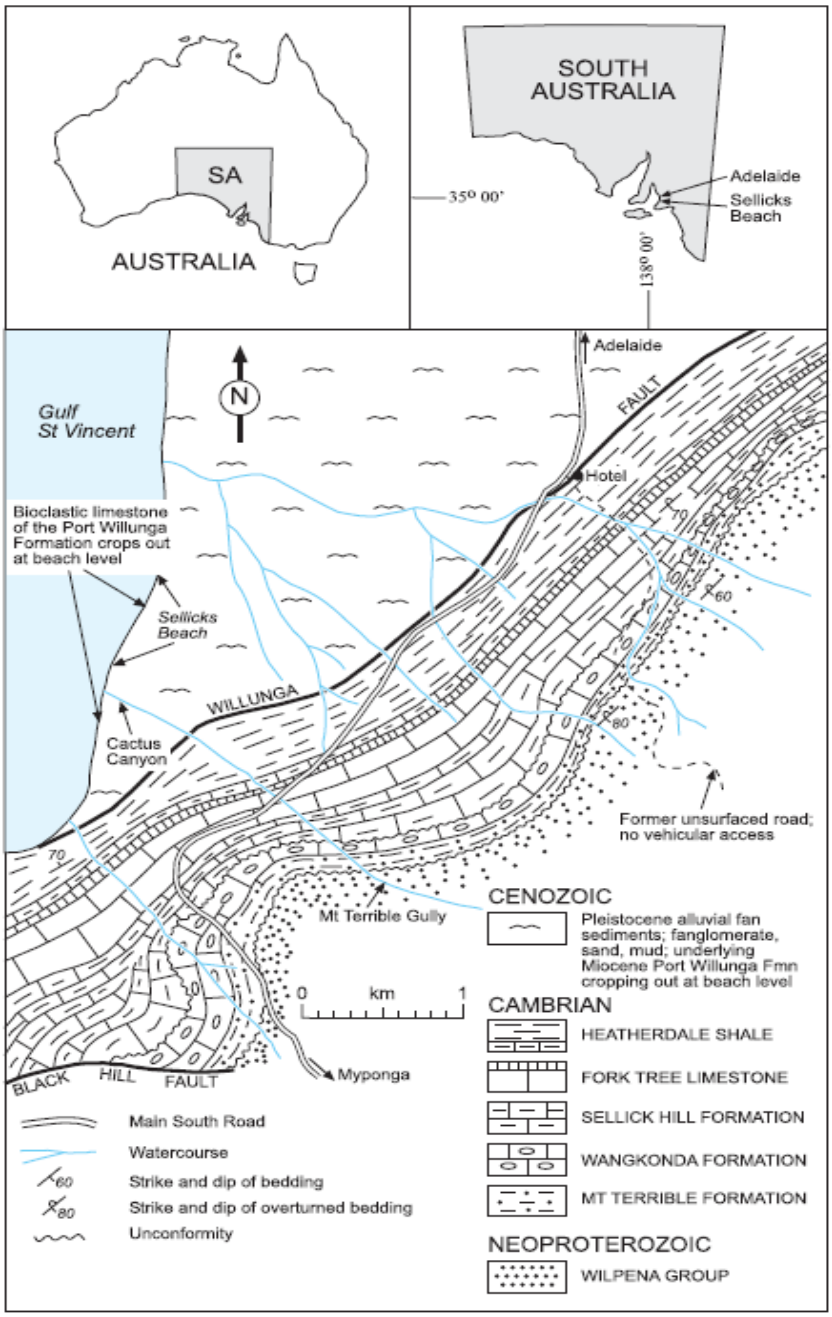

The field work started with a recognisance trip to Sellicks Beach where the main goal was to attempt to visually identify groundwater discharge zones. Colloquially known as water bubblers or seeps, and the discharging water at this sites is visible at low tide periods.

Figure 7 Map of the location of Sellicks Beach and its structural and geological features. After Cann et al. (2014).

During this recognisance trip a seep was identified (see Figure 8). Based on the location of this seep and the anecdotal information gathered, an area for the hydrogeological and geophysical surveys was delimited. The area of study identified is located in the southern part of Sellicks Beach (Figure 9).

Figure 8 Groundwater discharge zone identified in Sellicks Beach The discharge occurs as bubbling seeps (delimited in red).

Field work activities, followed during May 23rd to May 27th 2017, consisting of EC logging, water sampling during different parts of the tidal cycle and geophysical surveys.

3.2 Groundwater hydraulics and sampling

Three shallow piezometers were installed along a transect perpendicular to the shoreline from the cliffs of Sellicks Beach to the sea with a separation between piezometers of approximately 10 metres (Figure 9). EC loggers (*In situ* AquaTroll 200

non-vented data loggers) were installed inside the piezometers which had a short slotted screen interval of about 0.1 m in length. The loggers recorded temperature, pressure and EC, every minute from May 23rd in the morning to May 26th in the afternoon. It was not possible to install them at greater depth due to the presence of rocks (boulders and pebbles) at depth. Thereby piezo 3 was located closest to the cliffs, followed by Piezo 2 located 10 metres further towards the sea, Piezo 1 was located closest to the sea (Figure 9). Piezo 1 accesses the seep which was located during the first stage of the fieldwork activities (Figure 8).

Figure 9 Location of the 3 piezometers, at the southern part of Sellicks Beach.

Water samples were collected from the three piezometers, generally every 12 hours using a hand pump (see Table 2 for details). The sampling activity presented difficulties

associated to the high tide inundating the area of study, additionally during low tide Piezo 2 was not accessing water. The samples were analysed in the field using a handheld YSI multi-parameter instrument that measures *EC*, pH, dissolved oxygen and temperature.

In addition, the samples were filtered and stored for later analysis of the stable environmental isotopes, ^{18}O and ^{2}H. A binary mixing model is commonly used to explain geochemical variations in water (Sohn, 2005). Given this, the ratios of ^{18}O and EC were analysed in a mixing model to determine the proportions of the freshwater and seawater end-members. The data was modelled with a binary equation (see Equation 2) (U.S. Geological Survey, 2017) .

$$X_1 = (C_{mix} - C_2) / (C_1 - C_2) * 100 \qquad (2)$$

Where:

X_1= percentage of the proportion of end-member 1 (groundwater)

$\mathbf{C_1}$= concentration of end-member 1 (groundwater)

$\mathbf{C_2}$= concentration of end-member 2 (seawater)

$\mathbf{C_{mix=}}$ concentration of the water mixture

Equation 2, calculated the percentage of the groundwater end-member present in the samples collected from the three piezometers installed at Sellicks Beach.

Table 2 Schedule of the sampling activities. The dark blue colour represent the samples taken from piezo 1, the yellow colour from piezo 2, the red colour from piezo 3 and the light blue represents the seawater samples.

Sample ID	Day	Time	Sample ID	Day	Time
P1A	24/05/2017	9:45:00	P2F	25/05/2017	23:00:00
P1C	24/05/2017	19:30:00	P2G	26/05/2017	10:30:00
P1D	24/05/2017	22:30:00	P3B	24/05/2017	13:45:00
P1E	25/05/2017	10:05:00	P3C	24/05/2017	19:10:00
P1F	25/05/2017	23:00:00	P3D	24/05/2017	22:50:00
P1G	26/05/2017	10:30:00	P3E	25/05/2017	10:20:00
P2A	24/05/2017	9:45:00	P3F	25/05/2017	23:00:00
P2B	24/05/2017	13:45:00	P3G	26/05/2017	10:30:00
P2C	24/05/2017	19:20:00	Ocean A	24/05/2017	9:45:00
P2D	24/05/2017	22:40:00	Ocean D	24/05/2017	22:30:00
P2E	25/05/2017	10:10:00	Ocean F	25/05/2017	23:00:00

3.3 Geophysical survey

A grid comprising 20 transects was designed in the surrounding area of the seep. Nine transects of 50 metres length each were performed in the north-south direction. Eleven transects of 25 metres each were recorded along the east-west direction, see Figure 10.

The geophysical data was collected using a CMD-Explorer instrument (Figure 6) in a 'continuous measurement with GPS' setting, where the conductivity in mS/m, and the coordinates were recorded every second.

However, those coordinates were corrected after the survey, using the data collected with a differential GPS, also known as Real Time Kinematic (RTK) positioning system that provides centimetre level position accuracy (Trimble Inc, 2017).

After collection, the data was processed with the RES2DINVx64 software (Geotomo Software, 2013), that provides a 2D interpretation of electrical conductivity surveys . Raw data from the twenty 2D transect lines was integrated and processed within

RES3DINVx64 to obtain a 3D model of the electrical resistivity distribution in the subsurface.

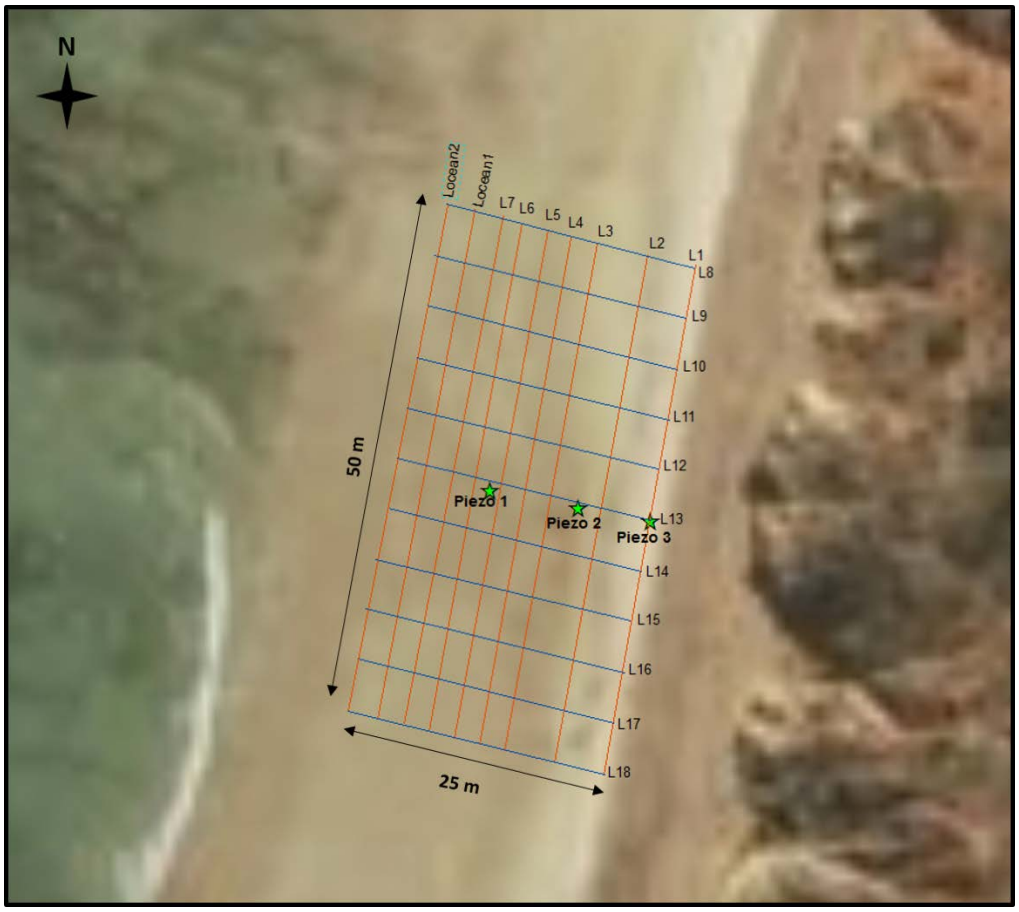

Figure 10 Schematic representation of the geophysical survey transect array at Sellicks Beach. The image shows the 11 x 50 m N-S transect lines (orange lines), the 9 x 25 m E-W transect lines (blue lines) and the three piezometers (green stars).

3.4 Thermal Imagery

In addition to the electrical resistivity survey, thermal imagery was taken using a handheld FLIR thermal camera. The FLIR camera takes visible light and thermal photos that show the temperature variations within the image frame. The survey was conducted at night, to avoid interference from solar radiation and was aimed at identifying differences in temperature associated with the presence of groundwater in contrast to sand and seawater.

Chapter 4

Results

4.1 Groundwater hydraulics

The results of the EC/water level /temperature loggers installed at Sellicks Beach are shown in Figure 11 and Figure 12. Figure 11 shows the temperature recorded from May 23rd at 11:30 am to May 26th 13:40 pm. The highest temperature was recorded by the logger installed in Piezo 1, displaying values ranging from 17 °C to 20.7 °C. Piezo 2 showed lower temperatures which ranged from 16 °C to 17 °C. During the night of May 26th temperatures dropped to 14 °C. Piezo 3 showed comparable results to Piezo 2, with temperature values ranging from 16 °C to 17 °C.

It should be noted that Piezo 1 was inundated by seawater during high tide, while Piezos 2 and 3 were only partially inundated over the tidal cycle. It is speculated that the presence of seawater was causing the temperature variations in Piezo 1 as shown in Figure 11.

As Piezo 1 was installed in the groundwater seep, the higher temperatures at this location can be associated with the discharging groundwater, compared to the lower temperature values displayed by Piezo 2 and 3 that can be related to the presence of seawater.

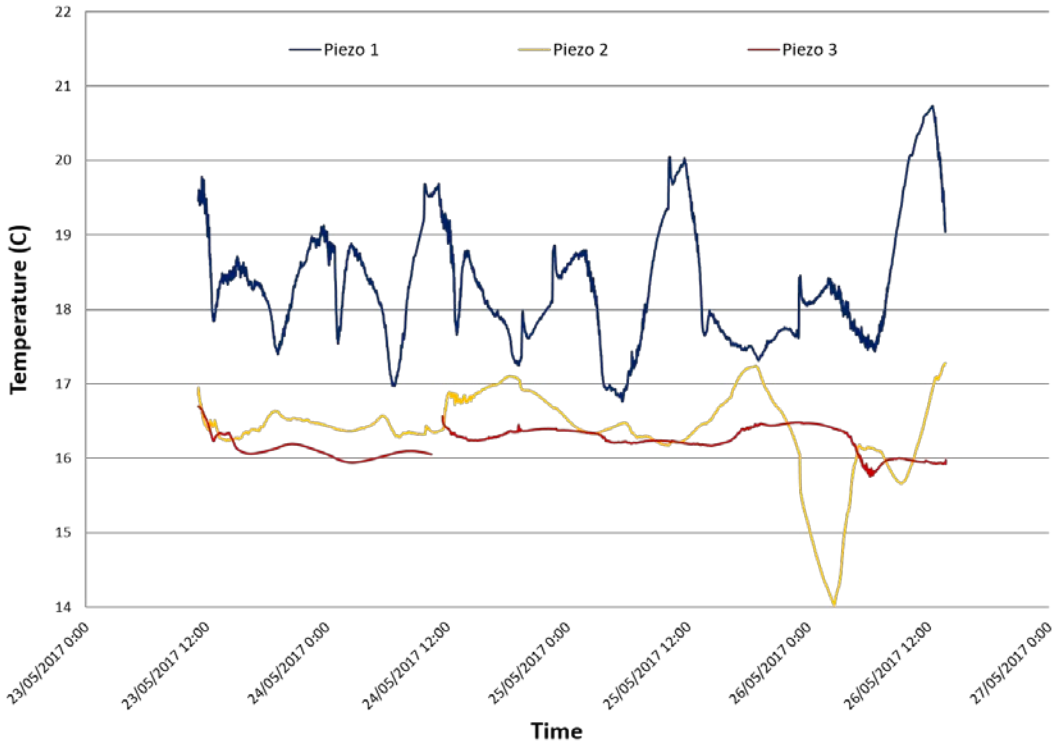

Figure 11 Continuous temperature data recorded at each of the three piezometers at Sellicks Beach from May 23rd at 11:30 am to May 26th 13:40 pm.

Water levels were recorded by the three loggers installed at Sellicks Beach and corrected to mAHD using the accurate RTK measurements at the top of casing of the piezometers, and are shown in Figure 12. The levels vary from -0.4 mAHD to a maximum level of about 1 mAHD. This level fluctuation correlates to the tidal cycle variations. The highest water levels are displayed by Piezo 1 and could be associated to the discharging groundwater in that location and the small variations registered (noisy peaks) during high tide periods are due to wave action as Piezo 1 becomes fully inundated. Even though Piezo 2 and 3 only get partially inundated, they are also affected by wave action.

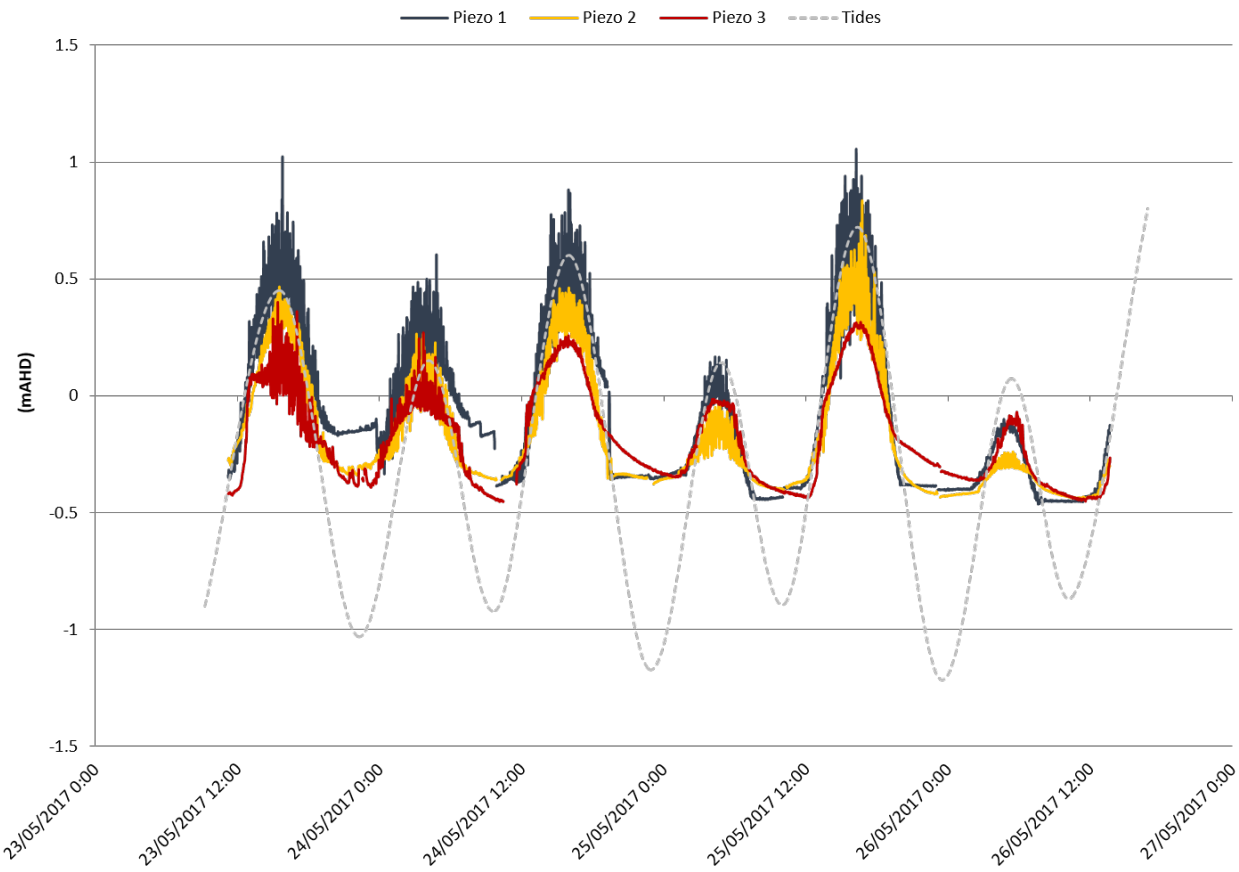

Figure 12 Water levels recorded in the three piezos at Sellicks Beach. The grey dashed line represents the tide level variations.

4.2 Hydrochemistry

The electrical conductivity (EC) results obtained onsite with the YSI multi-parameter meter are displayed in Table 3, where the less conductive values are from the samples taken at Piezo 1. The lowest value is from sample P1G (Piezo 1) with a conductivity of 20189 µS/cm taken at low tide during the morning of May 26th, and the highest value is from sample P3G (Piezo 3) with a conductivity of 58683 µS/cm collected onon the morning of May 26th at low tide conditions.

The samples collected from Piezo 1 with higher EC values (P1C and P1D) were taken at outgoing tide conditions, where the piezo was partially inundated with seawater. Samples P2A, P2f and P2G from Piezo 2 were not analysed with the YSI meter because

at the time of sampling the piezometer was dry due to the piezometer screen becoming clogged with sand.

EC results from Piezo 2 showed higher values compared to Piezo 1. The samples from Piezo 3 showed the most conductive values of the three installed piezos, where the highest value was more conductive than the seawater sample (Ocean F). This contrast in conductivity between the three piezometers suggests, that only Piezo 1 is intercepting groundwater, while Piezo 2 and 3 are influenced by seawater. This is consistent with the interpretation of the water level measurements (chapter 4.1).

Table 3 Stable Isotope data and EC from the samples collected at piezo1 (dark blue), piezo 2 (yellow), piezo 3 (red), ocean (cyan), and one of the seeps (green).

Sample ID	EC	$\delta^{18}O$	$\delta^{2}H$
	µS/cm	(‰, VSMOW)	(‰, VSMOW)
P1A	27657	-2.37	-13.27
P1C	54349	1.02	6.33
P1D	55804	-0.40	-1.55
P1E	26715	-2.81	-16.37
P1F	31844	-0.50	-2.64
P1G	20189	-3.64	-20.54
P2A	-	0.64	4.33
P2B	39071	1.11	6.60
P2C	34406	0.93	5.82
P2D	51050	0.46	2.45
P2E	54847	0.74	4.67
P2F	-	0.56	2.42
P2G	-	-0.62	-4.39
P3B	53071	1.14	6.51
P3C	37244	1.10	6.52
P3D	56092	0.93	4.96
P3E	48344	0.98	5.77
P3F	56415	1.00	5.89
P3G	58683	0.96	5.78
Ocean A	-	0.92	5.51
Ocean D	-	0.82	4.98
Ocean F	57040	0.59	2.37

Seep	-	-2.46	-15.22

Figure 13 and Table 3 show the stable isotope results. The ^{2}H and ^{18}O ratios of the three piezometers range from -20.54 to 6.59 ‰ VSMOW for ^{2}H and from -3.63 to 1.13 ‰ VSMOW for ^{18}O.

In accordance with the results of the water level measurements and EC readings, the ^{18}O and ^{2}H levels seem to suggest that Piezo 1, is the only piezometer accessing groundwater. Especially at low tide, samples in Piezo 1 show a more negative isotopic ratio and are closer to the meteoric water line, compared to Piezo 2 and 3. This suggests a meteoric origin of the water sampled at Piezo 1 during low tide periods.

The most enriched sample from Piezo 1 was taken during the outgoing tide when the piezo was partially inundated so we can infer by this and the EC values obtained with the YSI meter that the results of this sample are influenced by seawater.

The rain samples presented in Figure 13 are from rainfall events recorded from March to May 2017 and show depleted ratios similar to the values from Piezo 1. The precipitation ratios are in the range of -24.83 to -12.45 ‰ VSMOW for ^{2}H and -5.32 to -3.51 ‰ VSMOW for ^{18}O and are very similar to the isotopic ratios found for the seep. Overall, this confirms the meteoric origin of water in piezo 1. Samples from Piezo 2 and 3 display more enriched values and are similar to the isotope ratios of the seawater samples taken near the shoreline.

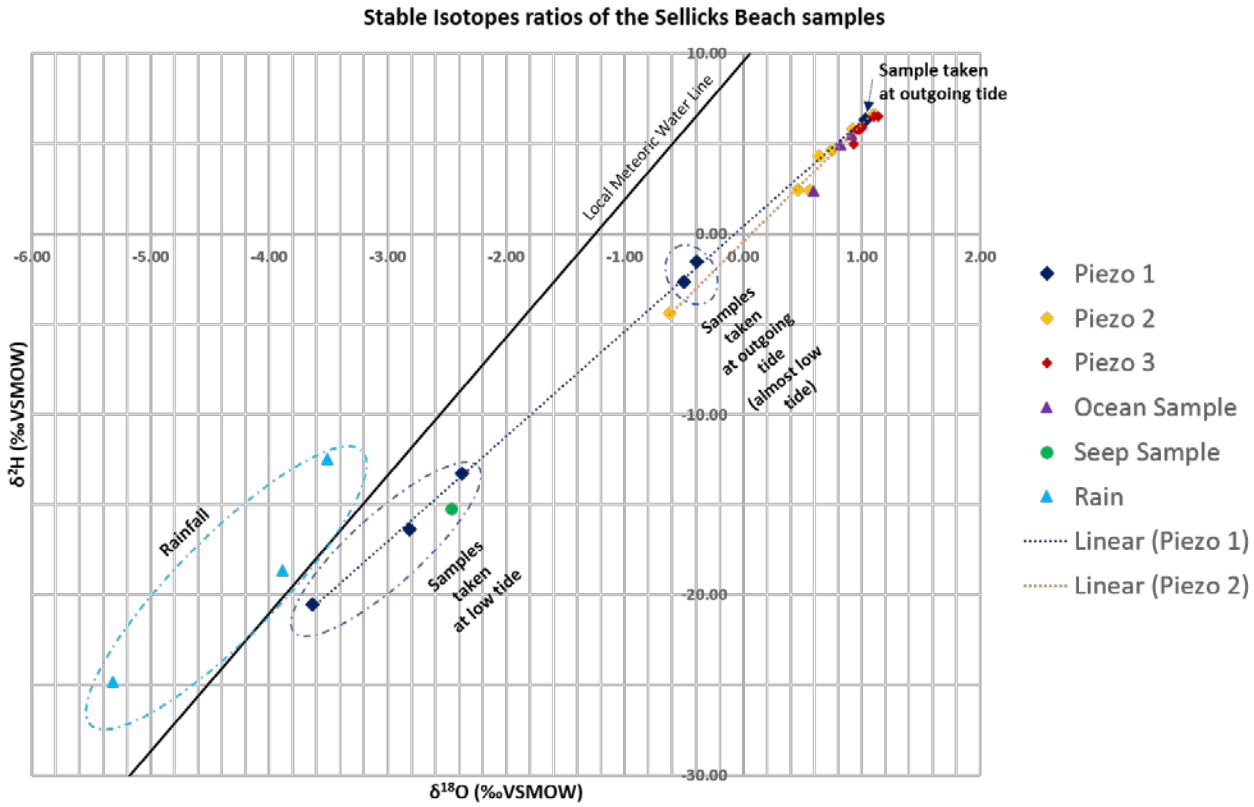

Figure 13 stable Isotopes (^{2}H and ^{18}O) ratios of the samples from the three piezometers, rainfall, seep and seawater.

Figure 14 shows the proportion of the groundwater end-member present in each sample using the EC results obtained with the YSI instrument and the stable isotope ^{18}O. The samples that show 100% of the groundwater component are P1A and P1G and where taken at low tide, presented low conductivity and more depleted values. Meanwhile sample P1F taken during low tide (almost at low tide) showed a different estimation from the two methods: ^{18}O values suggest a groundwater component of 40% within piezo 1, while the EC results would indicate a~90% groundwater component. It appears, that for this sample and most of the samples from Piezo 2 and 3, the EC values overestimated the groundwater component within the mixture.

In general, both ^{18}O and EC showed that most of the samples taken at Piezo 3, the groundwater component was contained less than 20% groundwater.

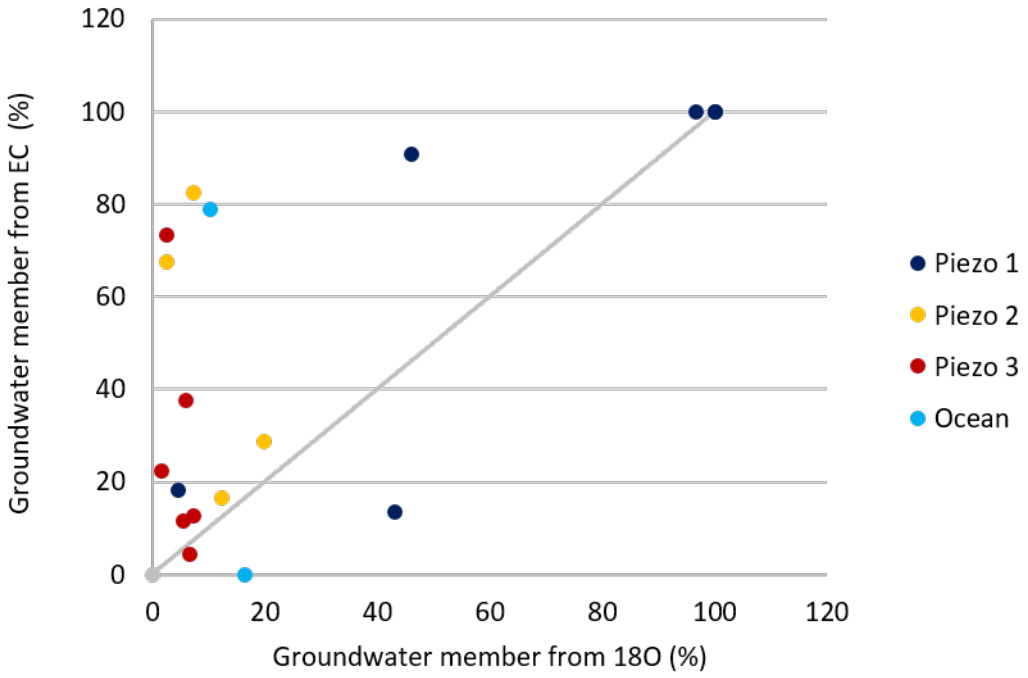

Figure 14 Two component mixing model using measured electrical conductivity and the stable isotope ratio 18O from the samples taken at Sellicks Beach.

The electrical conductivity results from the three piezos are presented only in Appendix 2, but are not considered for interpretation due the quality of the data registered.

4.3 Geophysical surveys

The results obtained by the electrical conductivity survey are presented below, and include 2D images and a 3D integrated multi-layer model. The conductivity results presented in this study were measured using the high depth configuration of the CMD-Explorer.

Figure 15 shows the apparent resistivity results obtained with the RES2DINV inversion program (Geotomo Software, 2013) of the transect line 6, that runs from north to south, intersecting Piezo 1 (Figure 10). At the margins of transect 6 less resistive values were identified (blue coloured), with ranges within 1 to 2 ohm.m. Figure 15 shows a zone of high resistivity in the centre of the transect which diminishes towards the edges. The

most resistive section (orange to purple) was about 7 metres long horizontally, and is visible in the centre part of the transect, and located at a depth of 2 to 5 metres, with values ranging from 6 to 9 ohm.m. This contrast in resistivity along transect 6 can be related to the presence of the groundwater seep in Piezo 1 showing higher resistivity and the salt content present in the sediments of the beach and in seawater that show lower resistivity values.

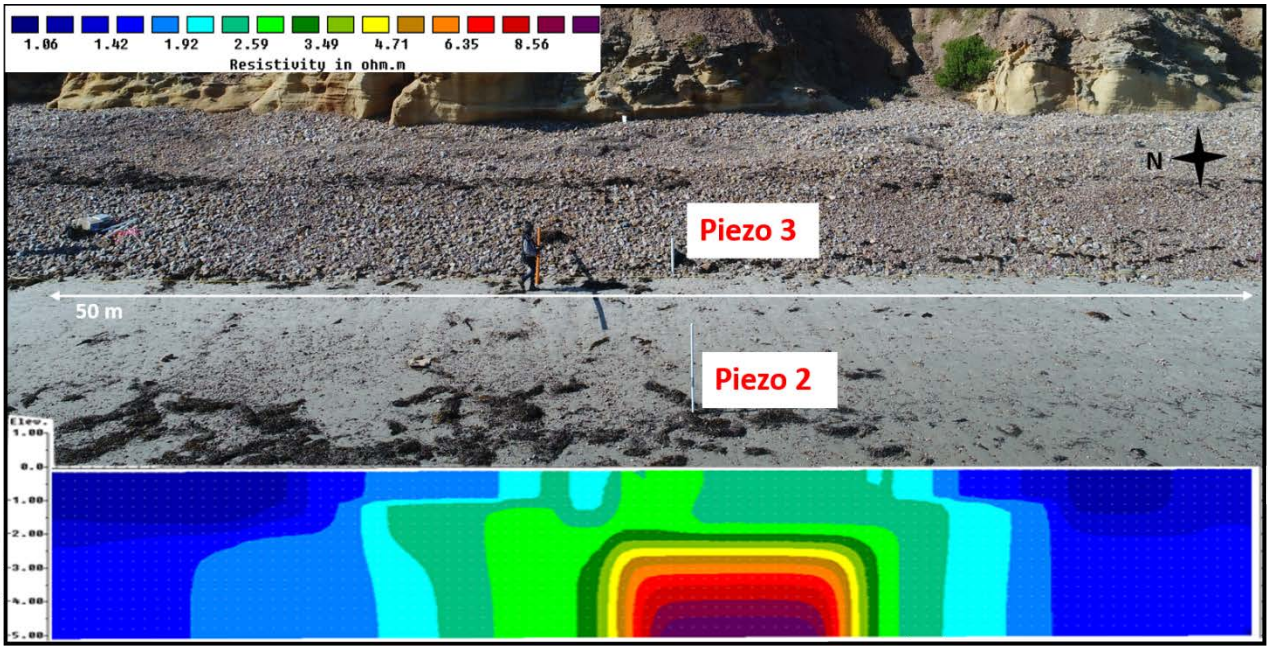

Figure 15 Aerial image taken above piezo 1, in the study area at Sellicks Beach. It is also included the 2D resistivity transect (see Appendix 1, transect 6) that runs from north to south and intersects piezo 1 (hidden by the 2D resistivity transect).

Figure 16 shows the resistivity results from transect 13 that went from the cliff to the sea, intersecting the three piezometers. The less resistive values are below piezo 2 and 3 (blue coloured) and ranged from 0.9 to 1.5 ohm.m. Resistivity started to increase mid-section of the transect and was about 9.5 metres long horizontally, reaching its maximum resistivity below Piezo 1 at a depth from 2 to 5 metres, with values ranging from 3 to 5 ohm.m. This high resistivity values are similar to the ones displayed in Figure 15 around the location of Piezo 1. The slightly lower resistivity detected in

transect 13 may be because the survey of both transects was made with about an hour of difference between each transect, making it possible for the composition of the groundwater present in Piezo 1 to change, and these small changes were sensed by this technique in both transects.

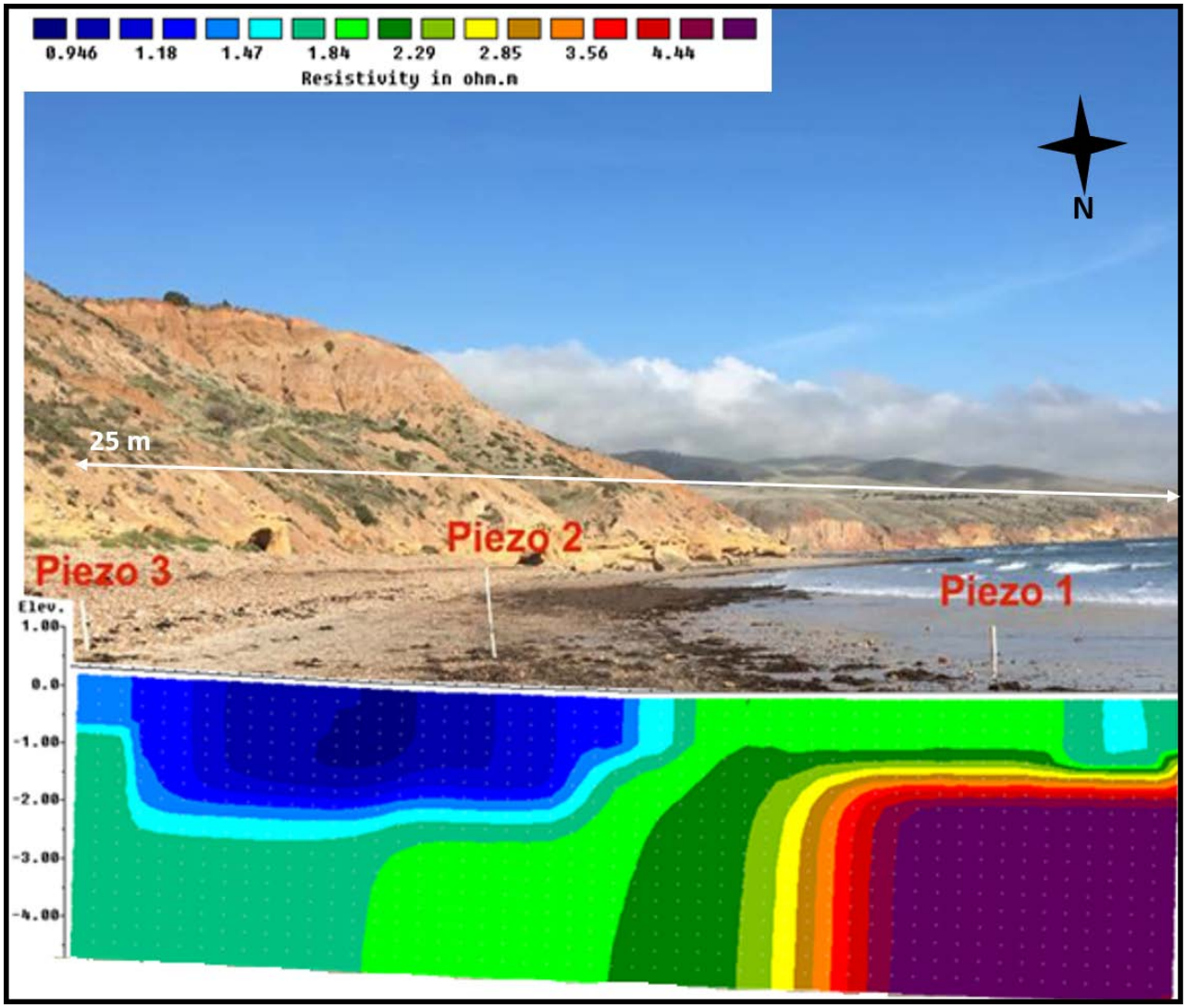

Figure 16 Image of the study area at Sellicks Beach. It is also included the 2D resistivity transect (see Appendix 1, transect 13) that runs from east to west and intersects all 3 piezos.

The twenty 2D transects were integrated and processed as a grid, with the interpolated resistivity results at nine different depths and are shown in Figure 17.

The shallowest layer located in the top left part of Figure 17 showed that the resistive values (red coloured) ranged from 4 to 6 ohm.m and have an approximate length of 10

metres. More specifically, the purple spot in the centre of the red zone in this layer represents a zone of high resistivity and is spatially situated in the same position as Piezo 1. This purple spot has a resistivity value of ~6 ohm.m and has an approximate length of 3 metres in the north-south direction. In contrast, the less resistive values are located along the northern part of the model and nearest to the sea (west area of the model). These value are within the range of 0.5 to 2 ohm.m. These conductive values can be associated with the high salt content of the seawater. Additionally the mustard colour (~2.8 ohm.m) present in most parts of the model could be related to the salt content in the sand of Sellicks Beach.

This multi-layer model shows that the low resistivity values associated to the presence of seawater tend to be less visible with increasing depth. In contrast, the length of the most conductive zone (red to purple coloured) tends to increase with depth, and shows a pattern that extends from the east (cliff side) to the west (sea side) of the model, indicating that groundwater flows towards the ocean and that a greater depths the groundwater component increases.

The integrated 3D model displayed in Figure 18 shows a similar electrical resistivity distribution compared to the multi-layer model of Figure 17. The lowest resistivity values (~0.1 ohm.m) are located in the western, northern and shallowest part of the model. While the most resistive values are located in the western-central part of the model (in the surroundings of piezo 1) with values of ~10 ohm.m.

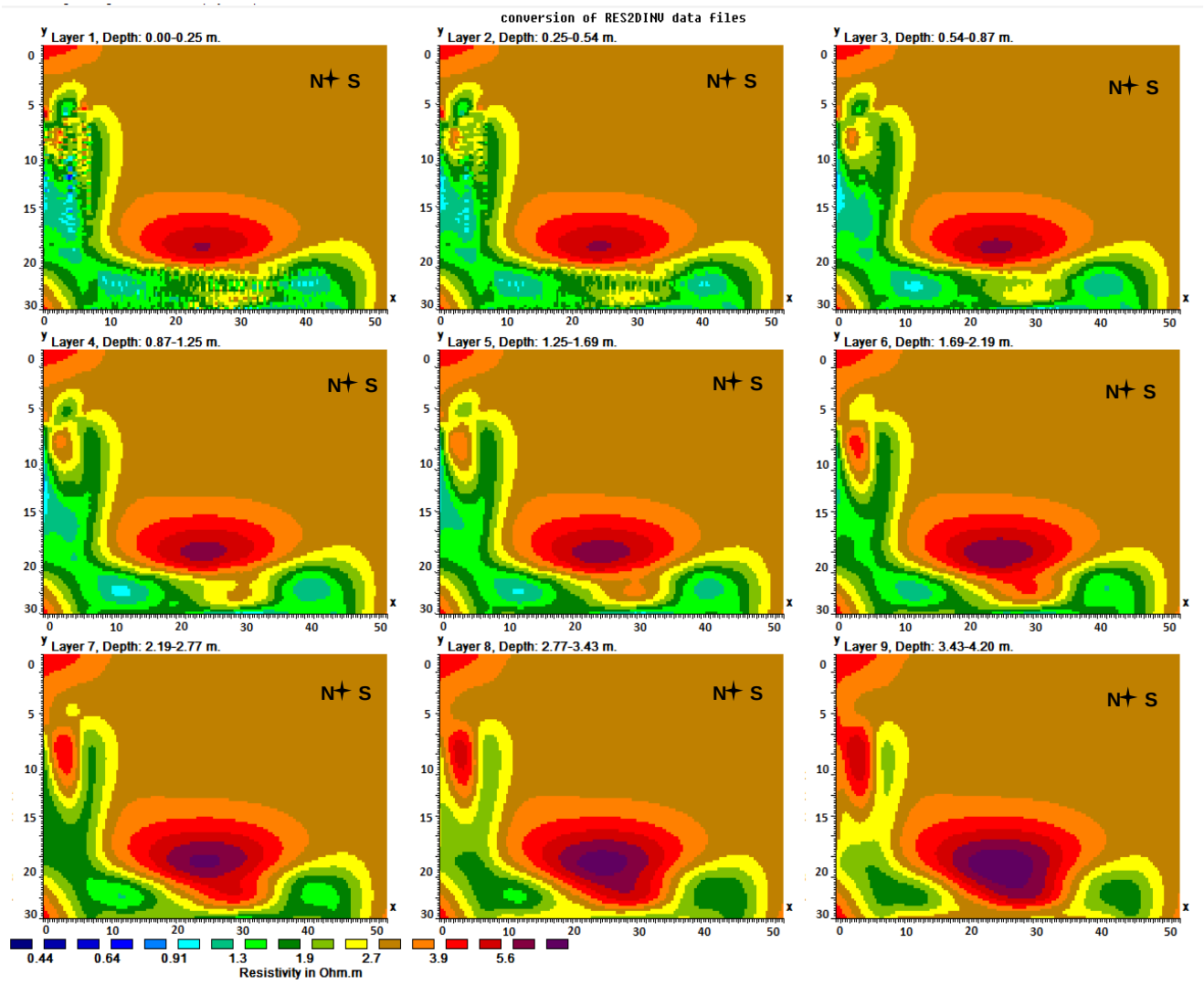

Figure 17 3D Multi-layer resistivity model of the integrated transects.

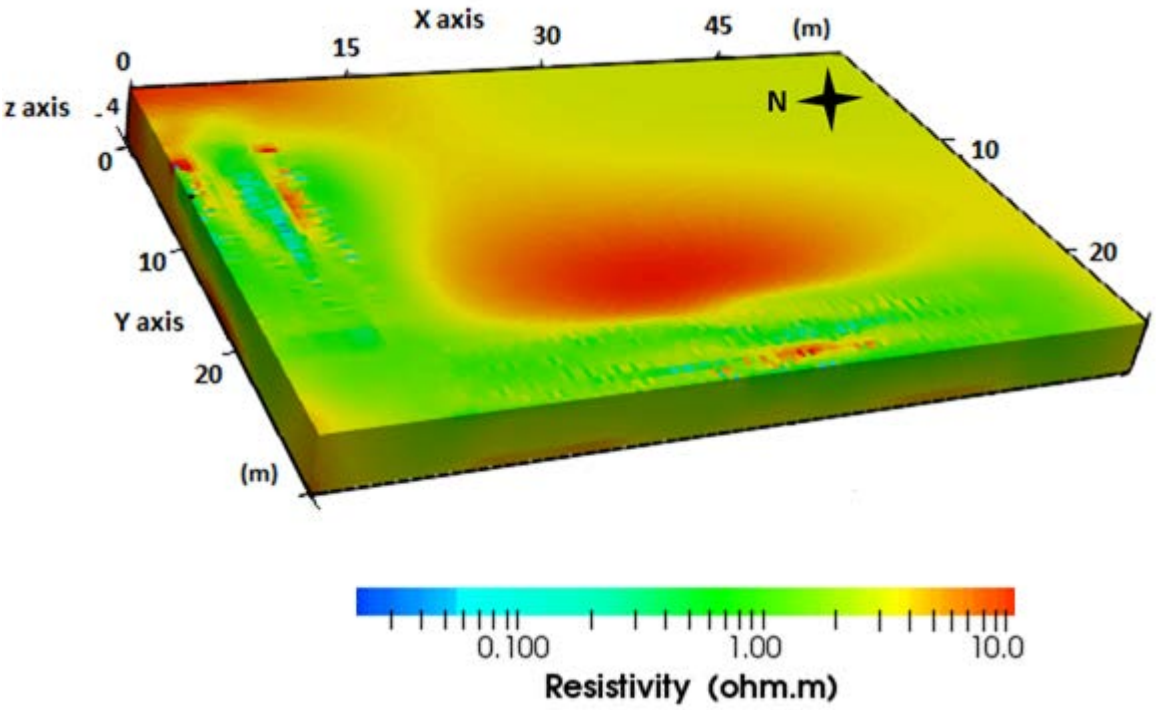

Figure 18 3D electrical resistivity model generated in Paraview with the inverted results obtained with Res3DINV.

4.4 Thermal images

Using the thermal camera, three seeps were located in the vicinities of the geophysical survey at Sellicks Beach and are shown in Figure 19. The results obtained with this method are presented in Figure 19, Figure 20, and Figure 21. Additionally, the location of the seeps is specified in Table 4.

Figure 19 shows the visible light and thermal photos of the Seep A. The area of seep A was ~50 x 60 cm and the temperature registered by the camera in the bubbling seep (dashed area in Figure 19) ranged from 17 to 19 °C, this valued contrast with the lower temperature of the sand in the surroundings and residual seawater.

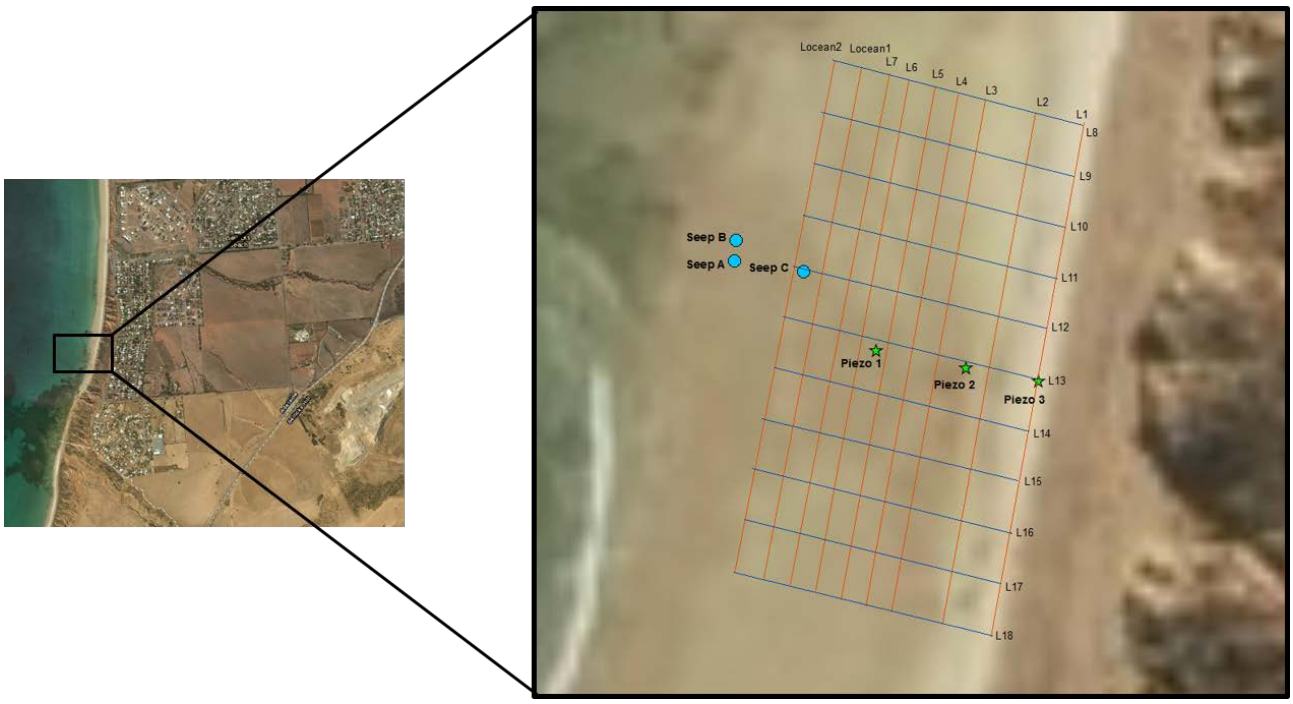

Figure 19 Location of the seeps identified with the thermal camera (light blue points), the piezometers (green stars) and the geophysical transect lines.

Table 4 Location and dimensions of the seeps identified with the FLIR camera.

Seep ID	Eastings	Northings	Elevation	Dimensions [cm]
Seep A	267866.2	6086636	-0.395	50 x 60
Seep B	267866.4	6086638	-0.371	30 x 25
Seep C	267872.9	6086635	-0.162	25 x 35

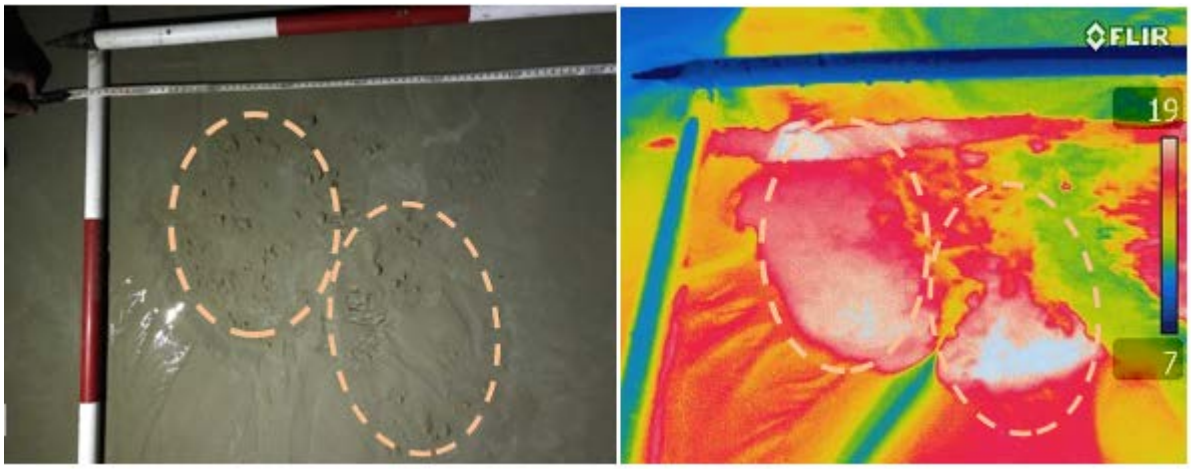

Figure 20 Visible light photo of seep A (left). Infrared photo of seep A, temperature in Celsius (right). The dashed ovals indicate the approximate area of the seep.

The infrared thermal mages from Seep B and C displayed in Figure 20 and Figure 21 respectively, were also able to identify the changes in temperature in the bubbling seeps in contrast to their surroundings. The temperature in seep B ranged from 17 to 19 °C and covered an area of ~30 x 25 cm. Meanwhile the temperature in seep C ranged from 16 to 18 °C, within an area of ~25 x 35 cm. The drain pattern of seep C was more diffused compared to seeps A and B.

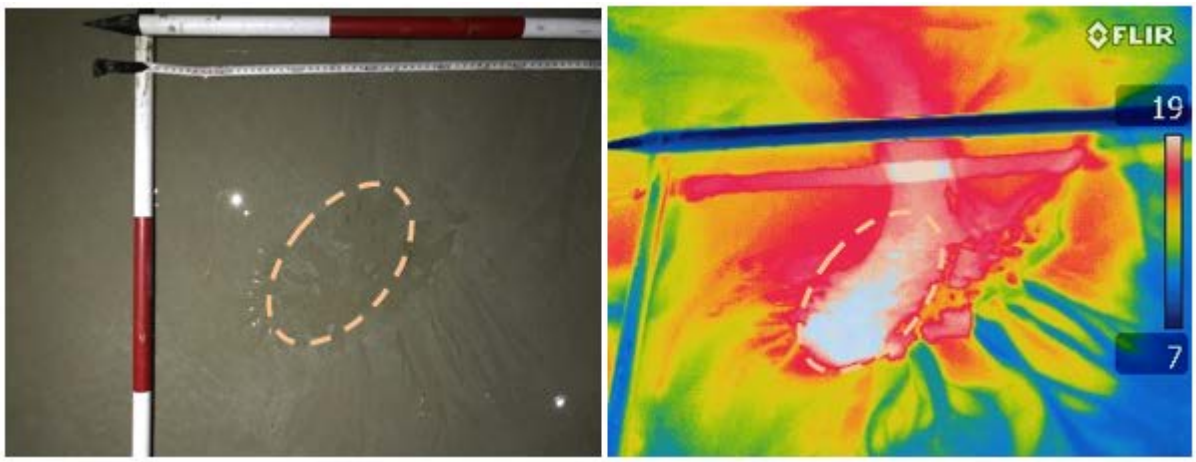

Figure 21 Visible light photo of seep B (left). Infrared photo of seep B, temperature in Celsius (right). The dashed ovals indicate the approximate area of the seep.

It is important to note that the temperature from the three seeps targeted with the thermal camera correlated well with the temperature registered by the Piezo 1 logger that ranged from 17 °C to 20.7 °C (shown in Figure 11).

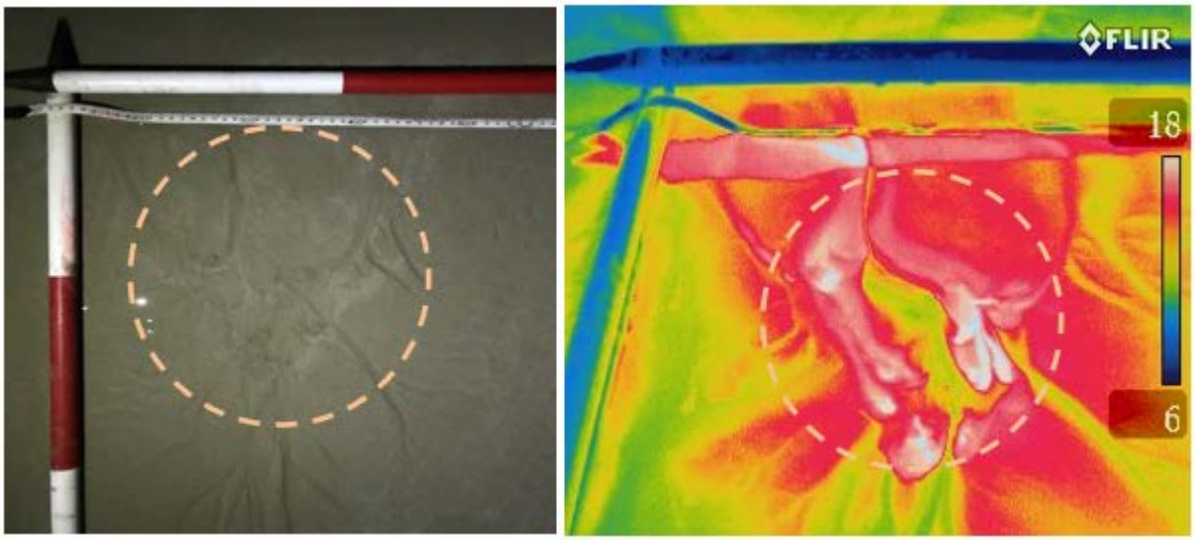

Figure 22 Visible light photo of seep C (left). Infrared photo of seep C, temperature in Celsius (right). The dashed ovals indicate the approximate area of the seep.

Chapter 5

Discussion

A multi technique survey was performed at Sellicks Beach in May 2017 to assess the CGD in the area. The survey comprised groundwater hydraulics, thermal imagery, hydrochemical and geophysical methods.

The 20 2D ground conductivity transect lines surveyed, were collated to create a multi-layer 3D model that showed the spatial distribution of the subsurface electrical resistivity in a 50 x 25 m grid. The electrical conductivity/resistivity of the ground is related to the water and soil chemical properties. The presence of ions, such as salts and other inorganic compounds, control the conductive behaviour in water. Water with high ion content tends to be more conductive, compared to water with less ions that shows a less conductive behaviour (Gianguzza et al., 2013). In the area of study where a piezometer (Piezo 1) was installed in a visible groundwater discharge site (seep), relatively high resistivities were recorded during the geophysical survey, with the area of elevated resistivity increasing with depth and spreading towards the sea. These higher resistivity values were associated with the location and plume of discharging groundwater.

The effect of tides was visible in the samples taken during mid and high tide periods, where the EC measurements were higher and the stable isotopes ratio (^{18}O and ^{2}H) was more enriched, compared to the low tide measurements that showed lower EC and more negative isotopic ratio. This results indicate the influence of seawater on the samples taken at mid and high tide. In addition, the binary mixing model calculated from EC and ^{18}O isotope data indicated that the groundwater component dominates the sample

composition taken at low tide at the location of Piezo 1 location. Meanwhile, in the samples taken at the locations of the other 2 piezometers (Piezo 2 and Piezo 3), the mixing model indicated a smaller contribution from the groundwater member, suggesting that at these locations little to no CGD was identified by this method. The results also suggested that when using the EC data, the binary mixing model tends to overestimate the groundwater component within the mixture in general.

The temperature data from the data loggers installed in the piezometers and also the handheld thermal imagery showed that the discharging groundwater has a higher temperature (average of 18.5°C), compared to lower temperature registered on the surface (sand and seawater), and also compared to the measured water temperature in the other 2 piezometers (average of 16.4 °C), that are believed were not accessing to groundwater. Moreover, the infrared thermal images were able to distinguish a preferential direction of the water flowing from the seeps. The temperature registered at the seeps ranged from 17.5 to 19 °C and flowed in a direction from inland towards the sea. The average dimension of the three discharging sites identified by the infrared thermal imagery was ~35 x 40 cm and is detailed in Table 4.

In general, the hydrochemical results obtained by the analyses of environmental isotopes, EC readings, and the temperature values from the piezometers, were able to identify the discharging freshwater in the area of study. Meanwhile the ground conductivity survey and the thermal imagery characterized the spatial distribution of groundwater.

Chapter 6

Conclusions

The objectives of this study were to identify coastal groundwater discharge (CGD) sites at Sellicks Beach, South Australia using different hydrogeophysical techniques, and to analyse their spatial distribution. Near surface geophysical methods demonstrated to be a valuable tool that can contribute to CGD identification. Ground conductivity investigations were used effectively to provide an image of the subsurface and identify the specific discharge location and extent of freshwater, as well as its preferential flowpath towards the sea at Sellicks Beach.

Infrared thermal imagery provided good results for assessing CGD at the surface and identified three freshwater discharge sites in the area of study, where their average dimensions was ~35 x 40 cm. The water temperature measured within the piezometers indicated that at the discharge site the temperature is higher (~18.5°C), compared to the temperature measured at the other two piezometer locations up-gradient of piezometer 1, where no discharge was visible (~16.4 °C). The temperature measured in the piezometer installed at the discharge site correlates with the temperature measured by the thermal camera which ranged from 17.5 to 19 °C. These temperature values were associated to freshwater.

The environmental isotopes analyses revealed that the water at the groundwater discharge site has meteoric origin. The EC measurements conducted at low tide indicated that, at the discharging site the water sampled comprises freshwater, meanwhile at mid to high tide periods, where the site gets inundated, the results are influenced by seawater.

Although the techniques used in this study are different, the results obtained are consistent and satisfied the main objective of this project by identifying the presence of CGD at Sellick Beach and showing its spatial distribution in the subsurface. The present study also demonstrated that the use of multiple techniques provides a good way to understand near surface water flow in coastal environments.

Recommendations

For future research, it is recommended to extend the duration of the hydraulic and hydrochemical measurements to investigate the temporal variability of the groundwater discharging sites at Sellicks Beach. To further identify discharging sites along the shoreline, it is suggested the use of aerial infrared thermal imagery that provides a broader view range compared to ground-based measurements. Non-invasive geophysical techniques that provide a larger depth of investigation, such as Transient Electromagnetic (TEM) methods, could be implemented to examine the vertical distribution of CGD and geological structures. Additionally, a quantitative assessment is recommended to estimate CGD fluxes in the area that help in the calculations of the discharge to the sea component of the Willunga Basin's water budget.

Appendix 1: Electrical resistivity transects.

- Transect 1

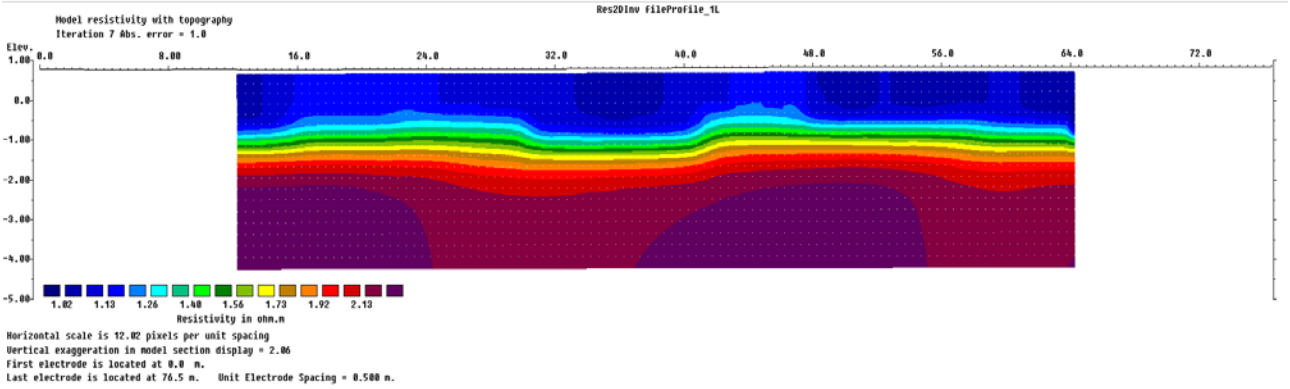

Figure A1.1. 2D resistivity transect line 1, which runs from north to south.

- Transect 2

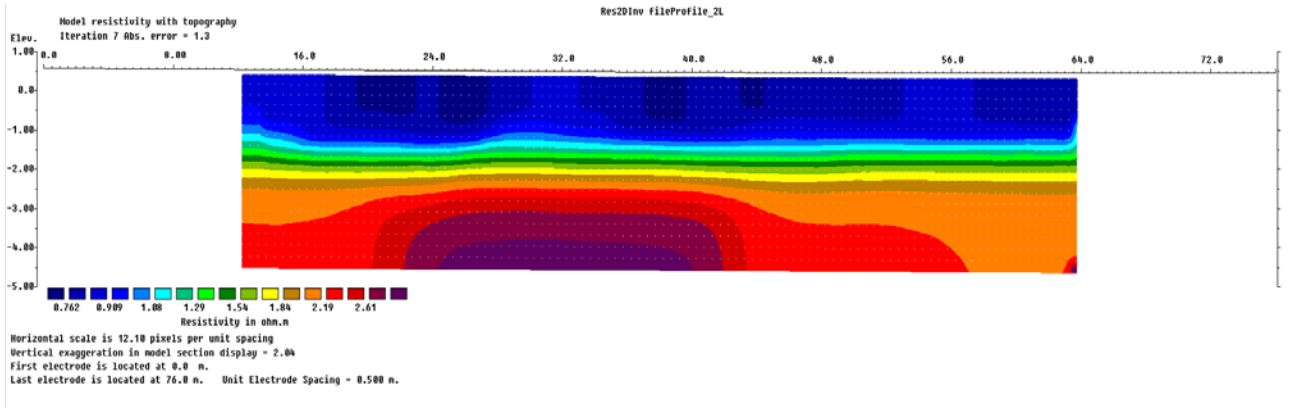

Figure A1.2. 2D resistivity transect line 2, which runs from north to south.

- Transect 3

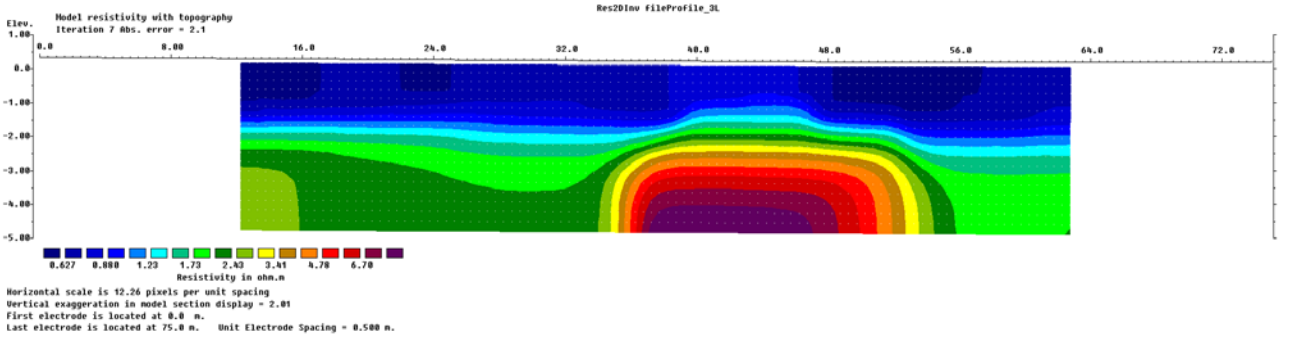

Figure A1.3. 2D resistivity transect line 3, which runs from north to south.

- Transect 4

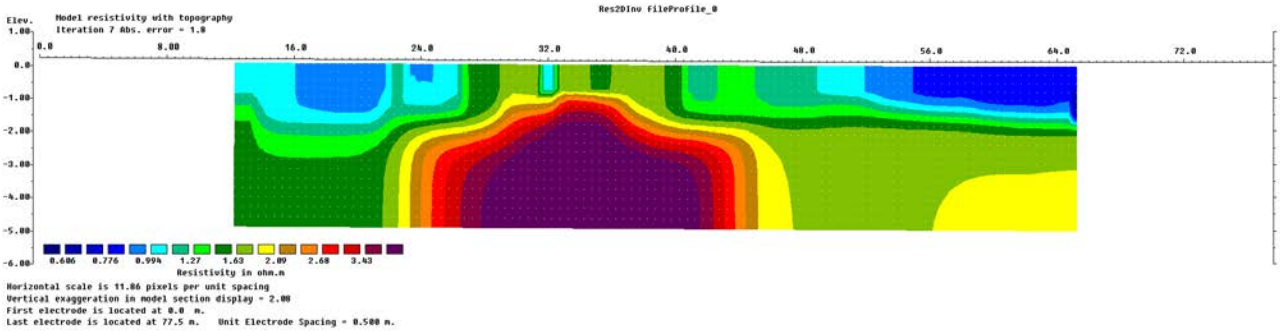

Figure A1.4. 2D resistivity transect line 4, which runs from north to south.

- Transect 5

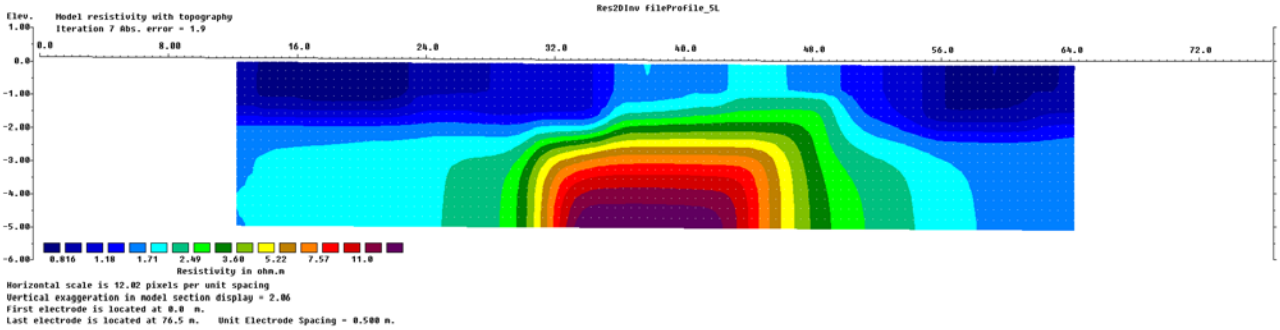

Figure A1.5. 2D resistivity transect line 5, which runs from north to south.

- Transect 6

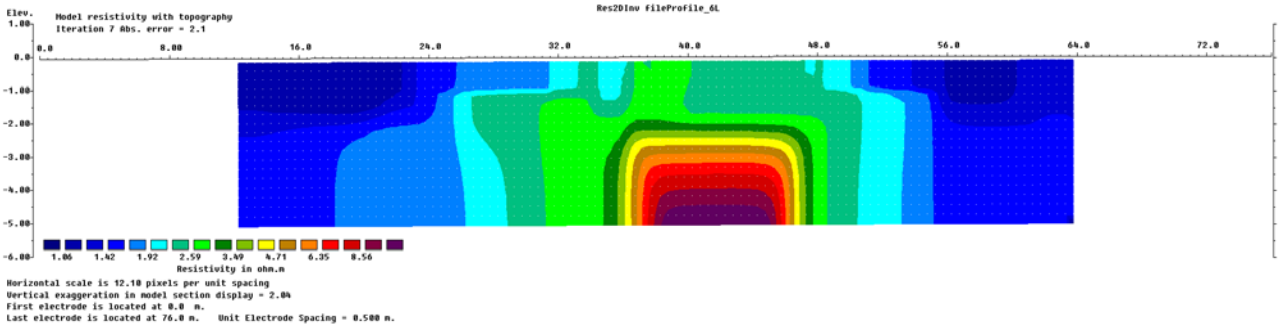

Figure A1.6. 2D resistivity transect line 6, which runs from north to south.

- Transect 7

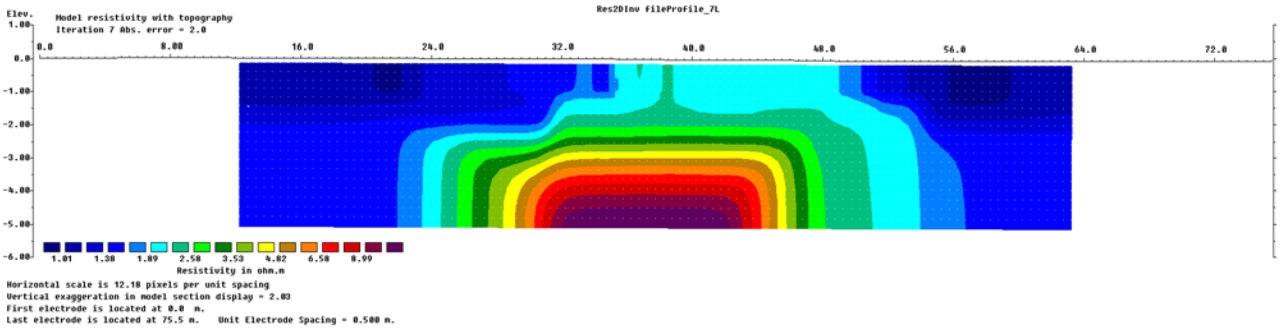

Figure A1.7. 2D resistivity transect line 7, which runs from north to south.

- Transect 8

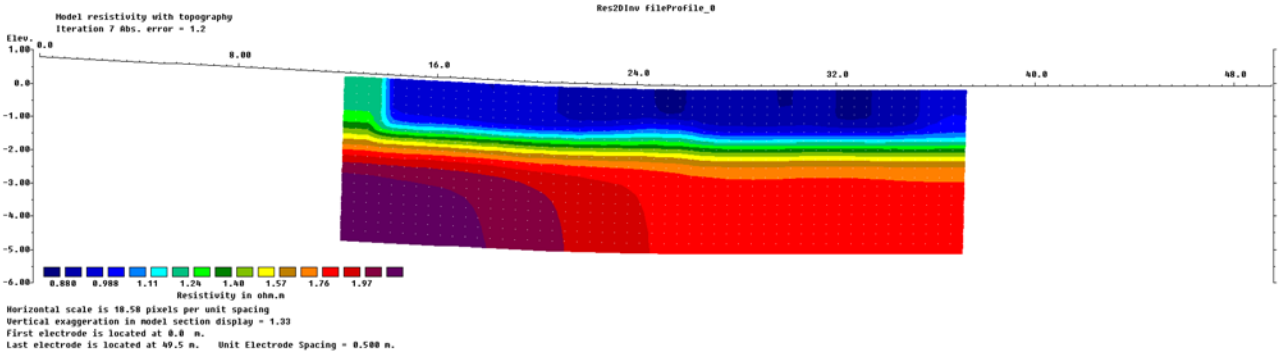

Figure A1.8. 2D resistivity transect line 8, which runs from east to west.

- Transect 9

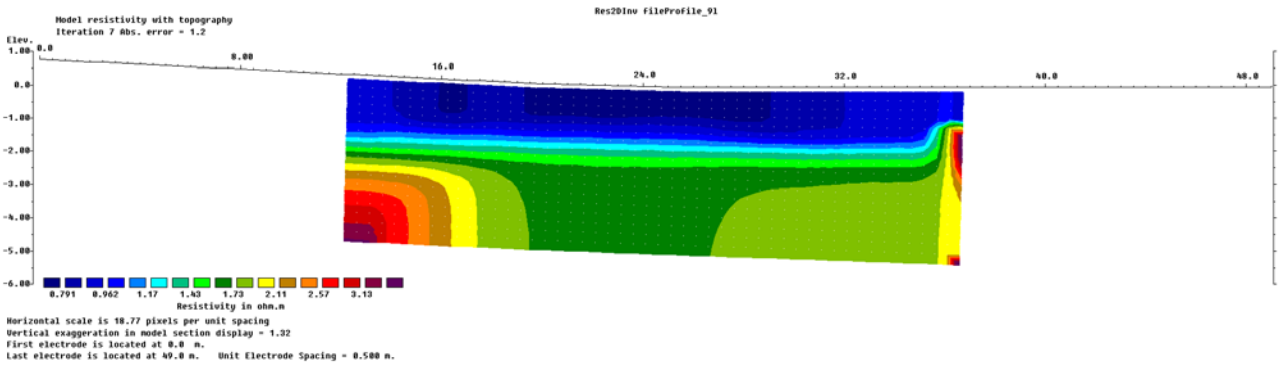

Figure A1.9. 2D resistivity transect line 9, which runs from east to west.

- Transect 10

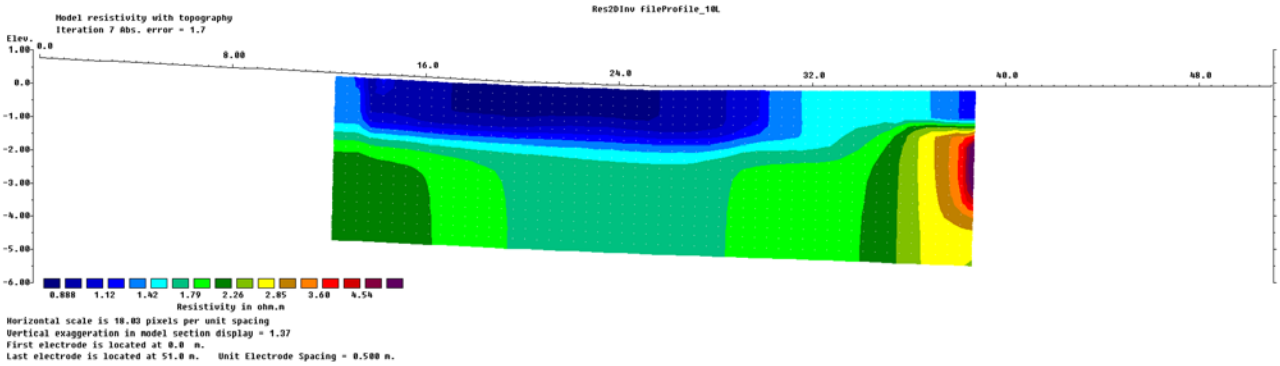

Figure A1.10. 2D resistivity transect line 10, which runs from east to west.

- Transect 11

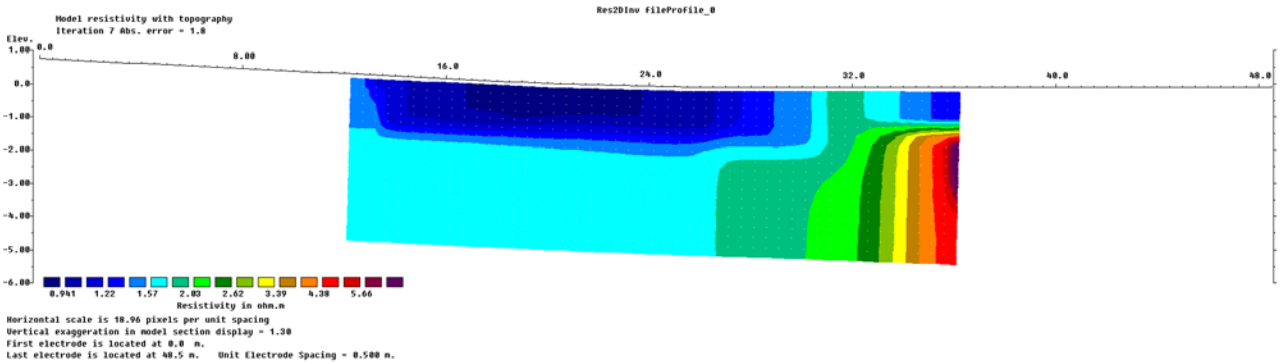

Figure A1.11. 2D resistivity transect line 11, which runs from east to west.

- Transect 12

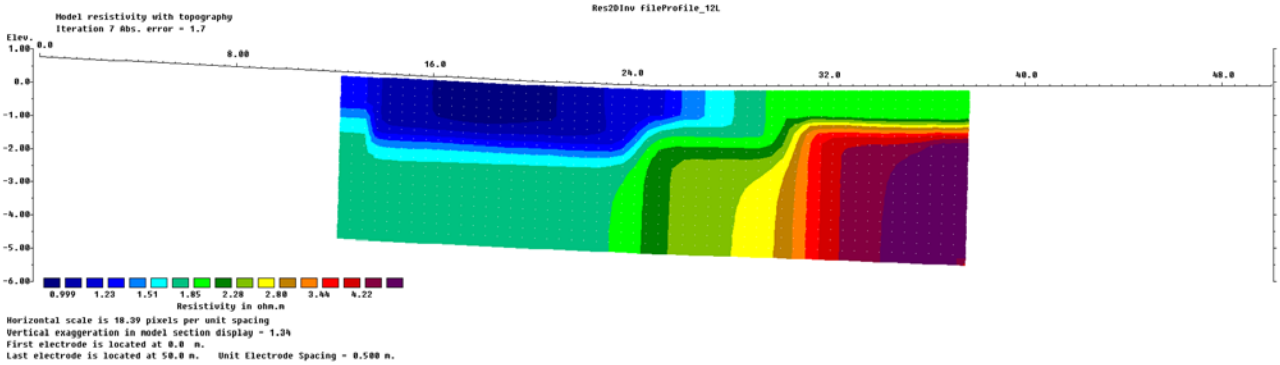

Figure A1.12. 2D resistivity transect line 12, which runs from east to west.

- Transect 13

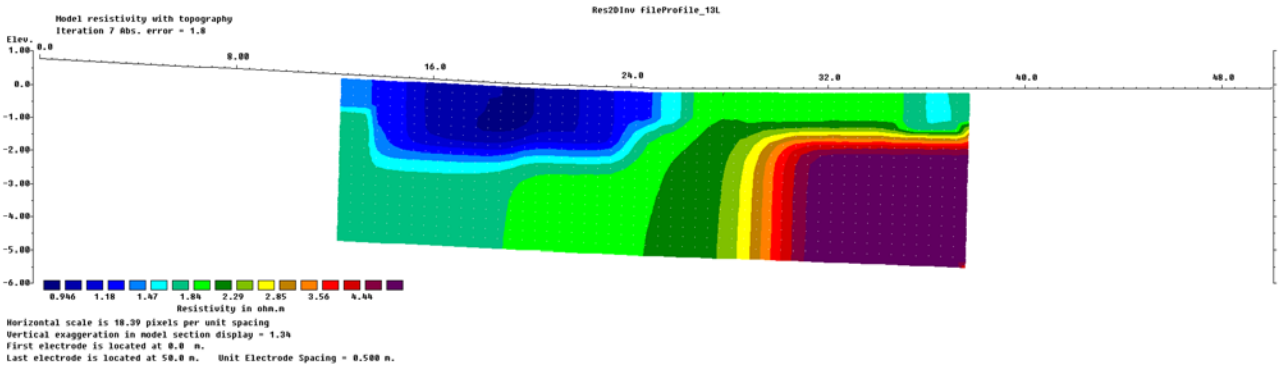

Figure A1.13. 2D resistivity transect line 13, which runs from east to west.

- Transect 14

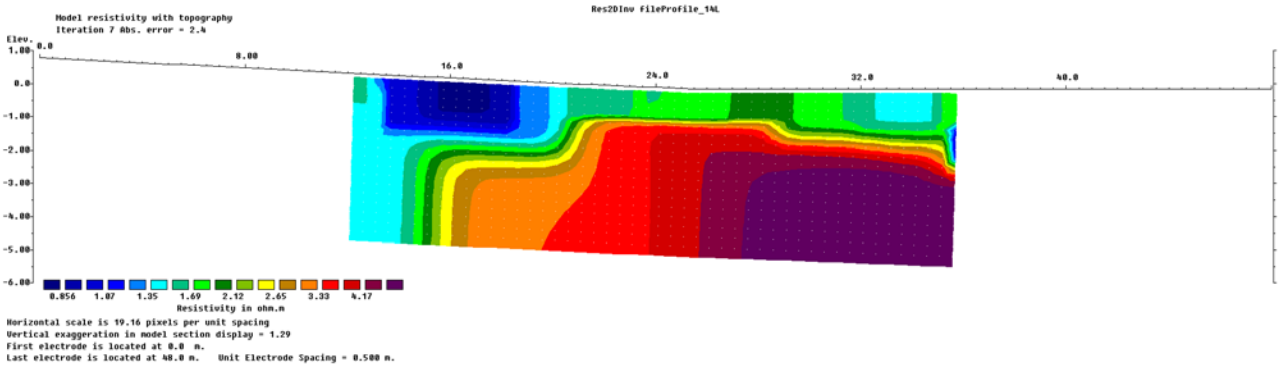

Figure A1.14. 2D resistivity transect line 14, which runs from east to west.

- Transect 15

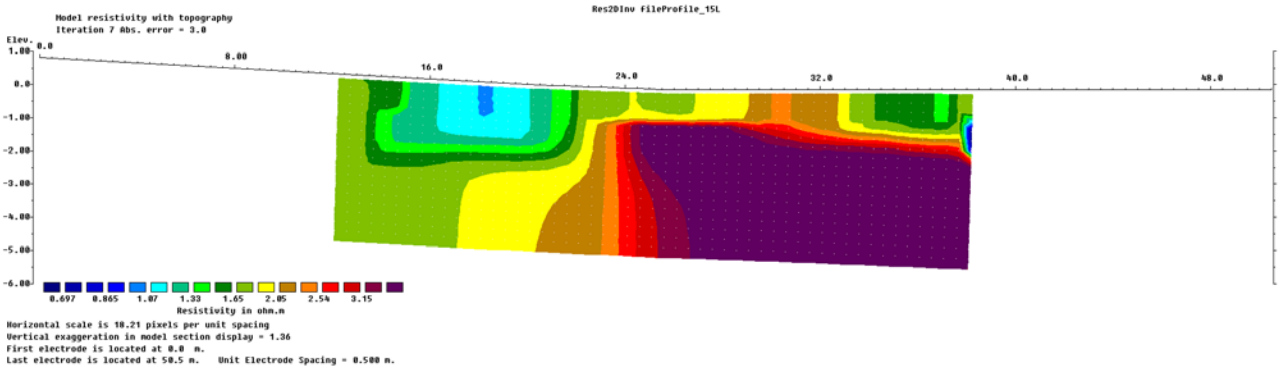

Figure A1.15. 2D resistivity transect line 15, which runs from east to west.

- Transect 16

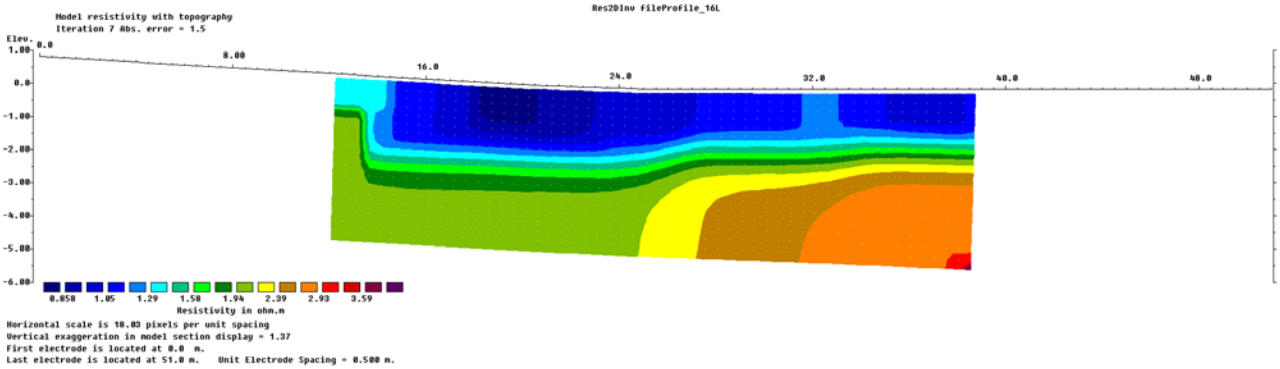

Figure A1.16. 2D resistivity transect line 16, which runs from east to west.

- Transect 17

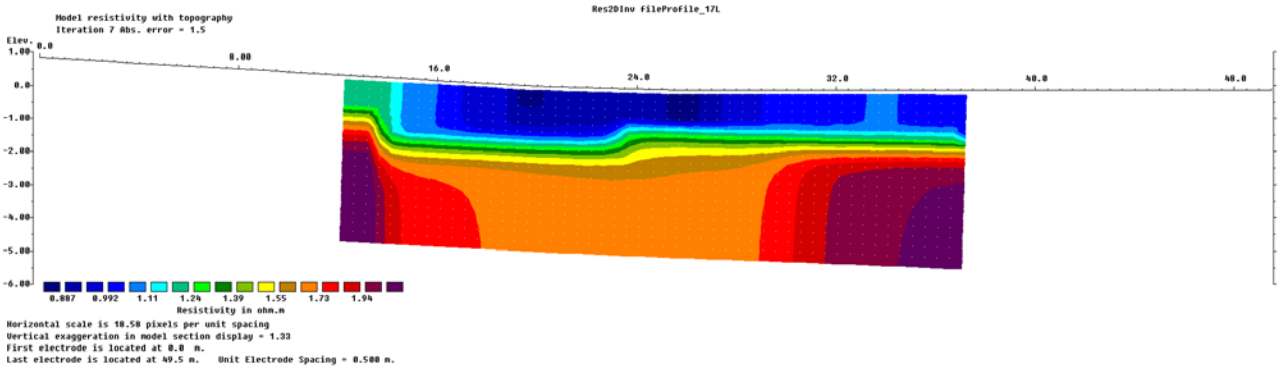

Figure A1.17. 2D resistivity transect line 17, which runs from east to west.

- Transect 18

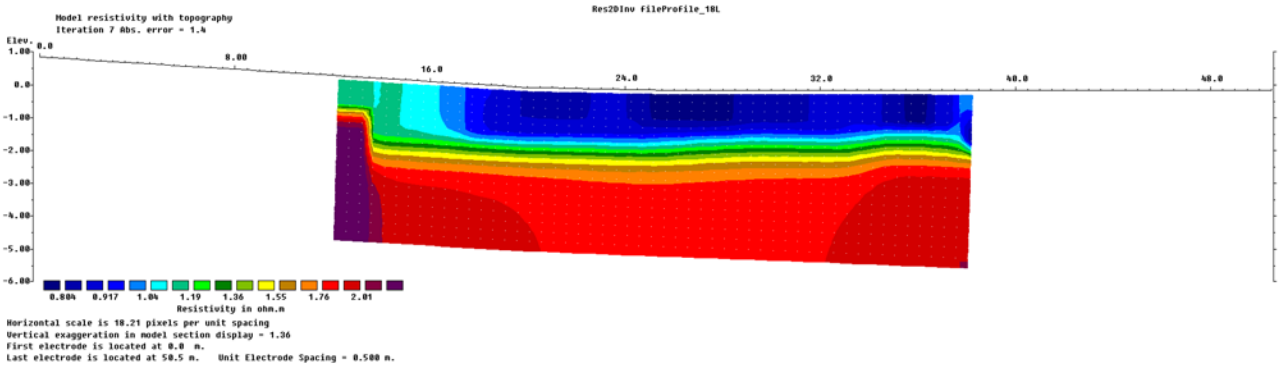

Figure A1.18. 2D resistivity transect line 18, which runs from east to west.

- Transect Ocean1

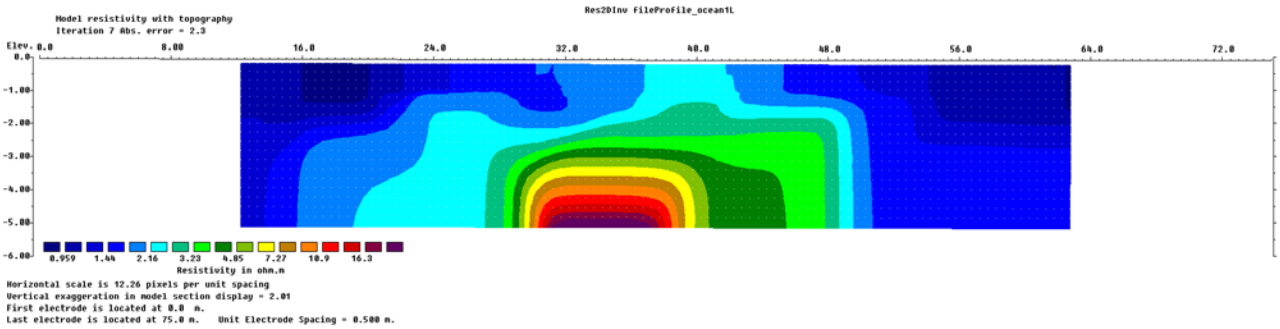

Figure A1.19. 2D resistivity transect line Ocean1, which runs from north to south.

- Transect Ocean2

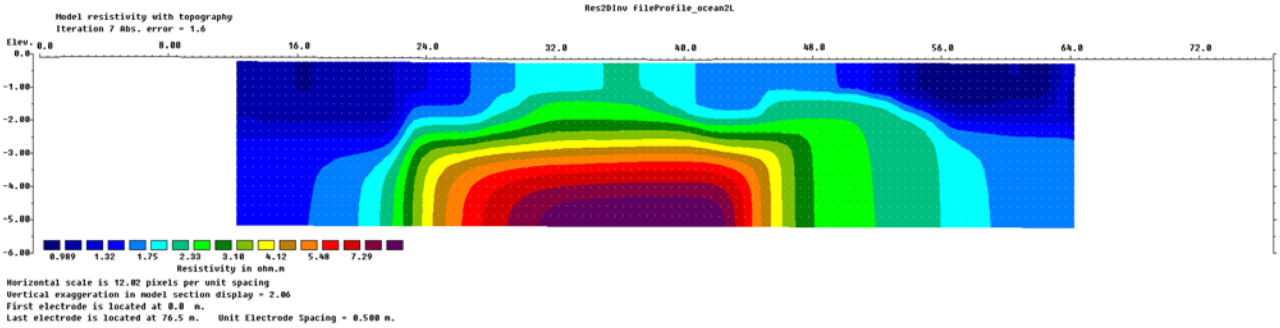

Figure A1.20. 2D resistivity transect line Ocean2, which runs from north to south.

Appendix 2: EC Measurements

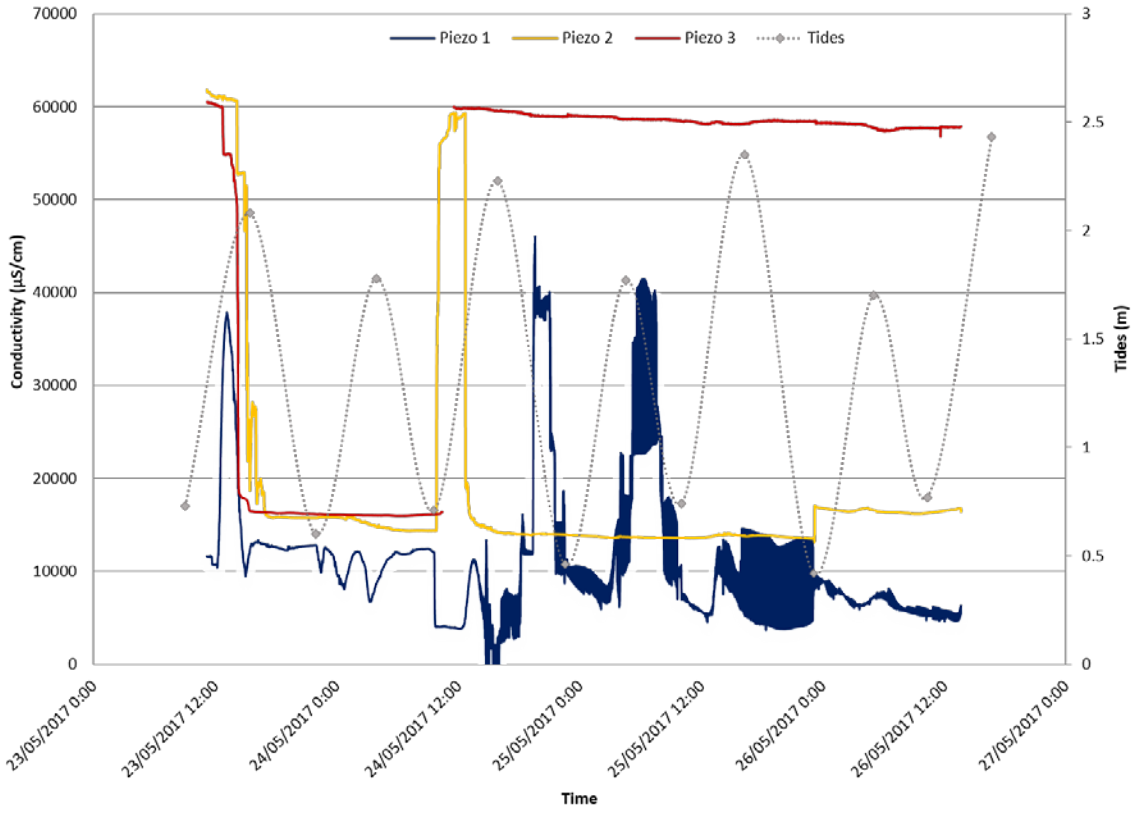

Figure A2.1. Electrical Conductivity recorded at each of the three piezometers at Sellicks Beach from May 23rd at 11:30 am to May 26th 13:40 pm.

References

Adelaide and Mount Lofty Ranges Nrm Board 2007, *Water Allocation Plan for the McLaren Vale Prescribed Wells Area* Government of South Australia.

Aggarwal, P, Froehlich, K, Gasse, V-W, Vienna, A, Kshitij, M & Kulkarni 2009, 'Environmental isotopes in groundwater studies', *In:* Silveira, L & Usunoff, EJ (eds.) *Groundwater*, EOLSS Publications.

Ataie-Ashtiani, B, Volker, RE & Lockington, DD 2001, 'Tidal effects on groundwater dynamics in unconfined aquifers', *Hydrological Processes* vol. 15, pp.655-669.

Bear, J 2007, *Hydraulics of Groundwater*, Dover Publications.

Bear, J & Verruijt, A 2012, *Modeling Groundwater Flow and Pollution*, Springer Netherlands.

Bourman, RP, Murray-Wallace, CV & Harvey, N 2016, *Coastal Landscapes of South Australia,* Adelaide, University of Adelaide Press.

Burnett, WC 1999, 'Offshore springs and seeps are focus of working group', *Eos, Transactions American Geophysical Union,* vol. 80, no.2, pp.13-15.

Burnett, WC, Aggarwal, PK, Aureli, A, Bokuniewicz, H, Cable, JE, Charette, MA, Kontar, E, Krupa, S, Kulkarni, KM, Loveless, A, Moore, WS, Oberdorfer, JA, Oliveira, J, Ozyurt, N, Povinec, P, Privitera, AMG, Rajar, R, Ramessur, RT, Scholten, J, Stieglitz, T, Taniguchi, M & Turner, JV 2006, 'Quantifying submarine groundwater discharge in the coastal zone via multiple methods', *Science of The Total Environment,* vol. 367, no.2, pp.498-543.

Burnett, WC, Bokuniewicz, H, Huettel, M, Moore, WS & Taniguchi, M 2003, 'Groundwater and pore water inputs to the coastal zone', *Biogeochemistry,* vol. 66, no.1, pp.3-33.

Butler, DK 2005, *Near-surface Geophysics,* United States of America, Society of Exploration Geophysicists.

Cann, JH, Lower, CS & Jago, JB 2014, 'Provenance and sediment characteristics of contemporary gravel deposits at Sellicks Beach, eastern shore of Gulf St Vincent, South Australia', *Australian Journal of Earth Sciences,* vol. 61, no.6, pp.819-836.

Church, TM 1996, 'An underground route for the water cycle', *Nature,* vol. 380, no.6575, pp.579-580.

Dfw 2011, *McLaren Vale PWA Groundwater Level and Salinity Status Report 2011*, Department for Water Government of South Australia.

Dyson, IA 1998, 'Estuarine facies of the North Maslin Sand and South Maslin Sand, Maslin Beach', *MESA Journal,* vol. 11, pp.42-46.

Fairburn, B 1998, 'The Willunga Embayment — an stratigraphic revision', *MESA Journal,* vol. 11, pp.35-41.

Geotomo Software 2013, *RES2DINV*.

Gf Instruments 2016, *Short guide for electromagnetic conductivity mapping and tomography*.

Gianguzza, A, Pelizzetti, E & Sammartano, S 2013, *Chemistry of Marine Water and Sediments*, Springer

Harrington, N & Cook, P 2012, *Willunga Research Update*, National Centre for Groundwater Research and Training.

Instruments, G 2016, *Short guide for electromagnetic conductivity mapping and tomography*.

Johannes, RE 1980, 'The Ecological Significance of the Submarine Discharge of Groundwater', *Marine Ecology-Progress Series,* vol. 3, pp.365-373.

Knight, RJ & Endres, AL 2005, 'An Introduction to Rock Physics Principles for Near-Surface Geophysics', *In:* Butler, DK (ed.) *Near-Surface Geophysics*, United States of America, Society of Exploration Geophysicists.

Lamontagne, S, Le Gal La Salle, C, Simmons, C, James-Smith, J, Harrington, N, Love, A, Smith, A, Hancock, G & Fallowfield, H 2005, *Estimation of groundwater and groundwater N discharge to the Adelaide Coastal Waters Study area*, Flinders Centre for Coastal and Catchment Environments Technical Report No. 4,Adelaide.

Li, H, Boufadel, MC & Weaver, JW 2008, 'Tide-induced seawater–groundwater circulation in shallow beach aquifers', *Journal of Hydrology,* vol. 352, pp.211-224.

Martin, RR 1998, *Willunga Basin – Status of groundwater resources*, Primary Industries and Resources South Australia,Adelaide.

Mcneill, JD 1980, *Electromagnetic terrain conductivity measurement at low induction numbers*, Geonics Limited,Tech. Note TN-6.

Mulligan, AE & Charette, MA 2006, 'Intercomparison of submarine groundwater discharge estimates from a sandy unconfined aquifer', *Journal of Hydrology,* vol. 327, no.3, pp.411-425.

Mundy, E, Gleeson, T, Roberts, M, Baraer, M & Mckenzie, JM 2017, 'Thermal Imagery of Groundwater Seeps: Possibilities and Limitations', *Groundwater,* vol. 55, no.2, pp.160-170.

Pfister, L, Mcdonnell, JJ, Hissler, C & Hoffmann, L 2010, 'Ground-based thermal imagery as a simple, practical tool for mapping saturated area connectivity and dynamics', *Hydrological Processes,* vol. 24, no.21, pp.3123-3132.

Post, VEA 2005, 'Fresh and saline groundwater interaction in coastal aquifers: Is our technology ready for the problems ahead?', *Hydrogeology Journal,* vol. 13, pp.120-123.

Post, VEA, Groen, J, Kooi, H, Person, M, Ge, S & Edmunds, WM 2013, 'Offshore fresh groundwater reserves as a global phenomenon', *Nature,* vol. 504, no.7478, pp.71-78.

Povinec, PP, Aggarwal, PK, Aureli, A, Burnett, WC, Kontar, EA, Kulkarni, KM, Moore, WS, Rajar, R, Taniguchi, M, Comanducci, JF, Cusimano, G, Dulaiova, H, Gatto, L, Groening, M, Hauser, S, Levy-Palomo, I, Oregioni, B, Ozorovich, YR, Privitera, AMG & Schiavo, MA 2006, 'Characterisation of submarine groundwater discharge offshore south-eastern Sicily', *Journal of Environmental Radioactivity,* vol. 89, no.1, pp.81-101.

Schuetz, T & Weiler, M 2011, 'Quantification of localized groundwater inflow into streams using ground-based infrared thermography', *Geophysical Research Letters,* vol. 38, no.3.

Short, MA, Lamontagne, S, Cook, PG & Cranswick, R 2014, 'Characterising the distribution of near-shore submarine groundwater discharge along a coastline using 222Rn and electrical conductivity', *Australian Journal of Earth Sciences,* vol. 61, no.2, pp.319-331.

Smith, ML, Fontaine, K & Lewis, SJ 2016, *Regional Hydrogeological Characterisation of the St Vincent Basin, South Australia: technical report for the National Collaboration Framework Regional Hydrogeology Project*, Record 2015/16, Geoscience Australia,Canberra.

Sohn, RA 2005, 'A general inversion for end-member ratios in binary mixing systems', *Geochemistry, Geophysics, Geosystems,* vol. 6, no.11.

Spies, BR & Eggers, DE 1986, 'The use and misuse of apparent resistivity in electromagnetic methods', *Geophysics,* vol. 51, no.7, pp.1462-1471.

Stieglitz, T 2005, 'Submarine groundwater discharge into the near-shore zone of the Great Barrier Reef, Australia', *Marine Pollution Bulletin,* vol. 51, no.1, pp.51-59.

Stieglitz, T, Taniguchi, M & Neylon, S 2008, 'Spatial variability of submarine groundwater discharge, Ubatuba, Brazil', *Estuarine, Coastal and Shelf Science,* vol. 76, no.3, pp.493-500.

Taniguchi, M, Burnett, WC, Cable, JE & Turner, JV 2002, 'Investigation of submarine groundwater discharge', *HYDROLOGICAL PROCESSES,* vol. 16, pp.2115–2129.

Telford, WM, Geldart, LP, Sheriff, RE & Keys, DA 1990, *Applied Geophysics*, Cambridge University Press.

Terwey, JL 1984, 'Isotopes in groundwater hydrology', *Challenges in African Hydrology and Water Resources (Proceeding of the Harare Symposium),* vol. 144, pp.155 160.

The Geological Society of Australia (Sa Division) 2014, *Sellicks Hill and Sellicks Beach Geological Trail* South Australia.

Trimble Inc 2017. *Precise Positioning Technology* [Online]. Available: http://www.trimble.com/unmanned/precise_positioning_technology.aspx [Accessed October 2017].

U.S. Geological Survey 2017. *Two-Component Mixing Equation for Investigating Sources of Recharge for a Well* [Online]. Available: https://oh.water.usgs.gov/tanc/tools/recharge_mixing_equations.html [Accessed October 2017].

Ward, SH & Hohmann, GW 1988, 'Electromagnetic Theory for Geophysical Applications', *In:* Nabighian, MN (ed.) *Electromagnetic Methods in Applied Geophysics: Theory*, Society of Exploration Geophysics.

West, GF & Macnae, JC 1991, 'Physics of the Electromagnetic Induction Exploration Method', *In:* Nabighian, MN (ed.) *Electromagnetic Methods in Applied Geophysics: Volume 2, Application, Parts A and B*, Society of Exploration Geophysicist

Yanful, EK 2009, *Appropriate Technologies for Environmental Protection in the Developing World: Selected Papers from ERTEP 2007, July 17-19 2007, Ghana, Africa*, Springer Netherlands.

Younger, PL 1996, 'Submarine groundwater discharge', *Nature,* vol. 382, no.6587, pp.121-122.

Zhdanov, MS 2002, *Geophysical Inverse Theory and Regularization Problems*, Elsevier Science.